

Analysis of fracture behavior of high-strength steels in tension after fire exposure



Wen-Yu Cai ^a, Jian Jiang ^b, Yan-Bo Wang ^{a,c}, Guo-Qiang Li ^{a,c,*}

^a College of Civil Engineering, Tongji University, Shanghai 200092, China

^b School of Mechanics and Civil Engineering, China University of Mining and Technology, Xuzhou 221116, China

^c State Key Laboratory for Disaster Reduction in Civil Engineering, Tongji University, Shanghai 200092, China

ARTICLE INFO

Keywords:

Fracture behavior
High-strength steel
Post-fire
Cooling method
SMCS model
Damage evolution law

ABSTRACT

High-strength steels have been widely applied in high-rise and long-span structures. Exposure to high temperatures due to fire may lead to reduction in material properties and fracture behavior of high-strength steels, greatly affecting the post-fire behavior of high-strength steel structures. This paper investigates the post-fire fracture behavior of high-strength steels in tension to pave the way for safety assessment of high-strength steel structures after fire. The fracture models of Chinese high-strength steels (Q460, Q550, Q690, Q890) and European high-strength steels (S460, S690 and S960) are calibrated and validated against limited experimental results of tensile coupon tests in an exposure temperature range of 200 °C to 1000 °C. The effect of air-cooling and water-cooling methods on the post-fire fracture behavior of high-strength steels is investigated. The fracture behavior is represented by the post-necking true stress-strain curve, toughness index (resistance to fracture initiation) in the stress modified critical strain model (SMCS) and damage evolution law. It is found that different types of high-strength steels with similar yield strength may exhibit quite different fracture behavior after exposure to high temperatures. The maximum exposure temperature and cooling method are two critical factors influencing the post-fire fracture behavior of high-strength steels. The true stress-strain curves after onset of necking can be simply expressed by a straight line with a slope, which becomes temperature dependent when the exposed temperature exceeding a critical level (e.g. 600 °C). The toughness index in SMCS model is subjected to great reduction in a temperature range of 800 °C to 900 °C for Q460-Q890 steels and 750 °C to 900 °C for S460-S960 steels. The most rapid evolution of damage occurs after being exposed to temperatures in a range of 650 °C to 900 °C. Compared to air-cooling method, the water-cooling method may lead to great reduction in the slope of post-necking true stress-strain curves (by 50%), significant reduction in toughness index (by 80%), and even change of fracture mode from ductile fracture to brittle fracture. It is recommended to choose reasonable and appropriate post-fire material properties for fracture prediction of different high-strength steels.

1. Introduction

Steel with a yield strength no less than 460 MPa is normally referred to as high-strength steel [1]. Due to the advantages of high strength and cost-effectiveness, high-strength steel has been increasingly employed in the key structural elements in engineering practice, such as tension members and connections in large space structures and columns in high-rise buildings [1,2]. However, high-strength steel is vulnerable to fire. After being exposed to fire, the material properties of high-strength steel such as strength, modulus and ductility may undergo a considerable change (decrease or increase) depending on the magnitude of exposed

temperatures and the cooling conditions [3]. According to the previous studies [3,4], the change in material properties of high-strength steels may be largely caused by their microstructural change during the heating and cooling phase in the fire event. The formation of martensite phase in high-strength steels may lead to an increase in strength but a decrease in ductility [3]. The increase in the ferrite and pearlite grain size may result in a decrease in strength of the high-strength steels due to the less hindrance provided by the grain boundaries to the motion of dislocation [4]. However, the change of the ferrite and pearlite size has limited effect on the fracture behavior and ductility for high-strength steels [4]. It was observed that the strength and fracture behavior of

* Corresponding author at: College of Civil Engineering, Tongji University, Shanghai 200092, China.

E-mail address: gqli@tongji.edu.cn (G.-Q. Li).

high-strength steels were also influenced by stress concentrations quantitatively measured by the stress triaxiality (the ratio of hydrostatic stress to von-Mises stress) [5]. Especially for the tension members, the stress triaxiality is normally very high in comparison to that for other structural members [5]. High stress triaxiality may increase the strength of high-strength steels by approximately 50%, however, it may decrease their ductility by nearly 75% [3,4]. After fire exposure, the high stress triaxiality combined with the formation of the martensite in high-strength steel tension members can lead to a significant reduction in their ductility and plastic strain at fracture initiation [3,5]. Owing to the change of strength and fracture behavior of high-strength steel tension members after fire, their overall deformation capacity may be overestimated. Therefore, to provide a guideline for safety assessment of high-strength steel tension members after fire, the post-fire fracture behavior of high-strength steel tension members need to be thoroughly investigated.

Previous research investigations suggested that, at elevated temperatures the strength and modulus of high-strength steels decreased with the increase of the exposed temperature [6–13]. However, after being exposed to a fire, the significant change of material properties of high-strength steels including strength, modulus and ductility has attracted more attention. Earlier studies on BS4360 43A steels [14] and S335J2H [15] demonstrated that mechanical properties of mild steels were not changed remarkably after being exposed to fire. When the maximum experienced temperature was more than 700 °C, the yield strength and tensile strength were subjected to no more than 20% reduction in comparison to their initial values, whereas the modulus can be even practically recovered after fire. For high-strength steels, changes of material properties after fire may be more considerable than that of mild steels [14]. Qiang et al. [16,17] conducted a series of experimental studies on post-fire mechanical properties of high-strength steels S460, S690 and S960 specified in European standard. It was found that the reduction in strength of high-strength steels after fire reached up to 50% when the experienced temperature was more than 600 °C, and high-strength steels exhibited ductile fracture behavior after fire and being cooled by natural air. Chiew et al. [18] found that RQT-S690 steel (reheated, quenched and tempered S690 steel) experienced a reduction in strength but minor increase in ductility when the experienced temperature was higher than 400 °C. According to Gunalan and Mahendran's study [19], the yield strength of high-strength steels G500 and G550 can recover 80% of their initial value after being exposed to 500 °C, While they may lose more than 20% of strength and modulus when the experienced temperature was more than 500 °C. Sajid and Kiran [3], Aziz and Kodur [20] and Lee et al. [21] found that the formation of martensite after fire exposure and high stress concentration may lead to a reduction in ductility for high-strength low-alloy steels such as ASTM A572 and A992. The above studies demonstrated that the degree of strength degradation of high-strength steels varied with the steel grades, however, these high-strength steels still exhibited ductile fracture behavior after fire.

The previous studies were merely based on the air-cooling condition, which is different from the reality of being cooled by water from sprinklers or firefighters. For mild steels, studies on Q235 [22,23], Q345 [22], ASTM 36 [24] suggested that water cooling may result in a reduction of ductility of mild structural steels due to the formation of martensite during the heating and cooling phases. The effect of cooling method on ductility of high-strength steels were also investigated. Wang et al. [25] found that air-cooling method can increase the ductility of Q460 steel when the experienced temperature was higher than 700 °C, whereas with the same experienced temperature the water-cooling method may lead to a reduction in the ductility of Q460 steel. The cooling method had a similar effect on Q690 steels [26–28]. Azhari et al. [29] found that the cooling method affected the ductility of G1200 steels and the effect varied with the steel grades.

Previous experimental studies mainly focused on the post-fire strength of high-strength steels and limited studies were on their post-

fire ductility. Besides experimental studies, numerically analysis is an effective way to determine the fracture behavior and deformation capacity of structural members. To numerically analyze fracture behavior of high-strength steel tension specimens after fire needs ductile fracture criterion or model. Several fracture models have been developed to numerically predict the ductile fracture behavior of steels, including McClintock model [30], Rice-Tracey model [31], Hancock-Mackenzie model [32], Cockcroft-Latham model [33], Gurson model [34], Johnson-Cook model [35], Wierzbicki model [36], Void Growth Model (VGM) and Stress Modified Critical Strain Model (SMCS) [5]. According to these models, plastic strain at fracture initiation is an index of fracture behavior of ductile material. When the material is mainly in tension, fracture plastic strain is mainly affected by stress triaxiality. By performing curve fitting for the stress triaxiality and corresponding fracture plastic strain of different ductile metals, it was found that fracture plastic strain was exponentially correlated to stress triaxiality [32,35,5,37]. Using previously developed models, fracture behavior of structural members made of high-strength steels such as Q460 [37,38], Q690 [1,39], S960 [40] was investigated and the corresponding fracture model parameters were calibrated for these high-strength structural steels. It was found that the previous developed fracture model can reasonably predict ductile fracture behavior of high-strength steels and the fracture properties varied with the categories of steels. However, the focus of these numerical studies was mainly on the fracture behavior of high-strength steels before being exposed to high temperatures, research on post-fire fracture behavior of high-strength steels is lacking [39], which pose difficulty for the safety assessment and design of high-strength steel members after fire.

This paper presented the numerical investigation of fracture behavior of high-strength steels with a yield strength ranging from 460 MPa to 960 MPa after being exposed to temperatures ranging from 200 °C to 1000 °C. The fracture analysis was first conducted for Chinese Q690 steel with a yield strength of 690 MPa. Using both experimental data and finite element analysis, the post-necking material properties for Q690 steels after fire based on air-cooling and water-cooling methods were obtained and validated, including true stress-strain curves extending beyond necking, the stress modified critical strain model (SMCS) and damage evolution law. Based on the validated approach, the true stress-strain curves, fracture model parameters and damage evolution law of the other categories of high-strength steels including Q460, Q550, Q890, S460, S690 and S960 after fire were determined. Finally, a validated ductile fracture model together with the calibrated parameters was proposed for the numerical prediction of post-fire fracture behavior of different high-strength steels.

2. Prediction of post-fire fracture behavior for Q690 steels

The prediction of post-fire fracture behavior of high-strength steel tension specimens needs accurate material properties including yield strength, elastic modulus, true stress-strain curves before and after onset of necking, fracture model (fracture initiation criterion) together with material-dependent parameters and damage evolution law which is used to mathematically describe the development of damage caused by fracture initiation and propagation. Since post-fire yield strength and elastic modulus of different types of high-strength steels have been thoroughly investigated in the previous studies [25–29], this section focuses on the post-fire material properties of Q690 steels after onset of necking.

2.1. Test specimen and finite element model

Test results of standard tension specimens made of Chinese Q690 steel (yield strength of 690 MPa) from Zhou et al. [26] were used to develop post-necking material properties for the fracture analysis. The specimen was designed and tested based on the Chinese standard [41]. Before the tensile test, the tension specimen shown in Fig. 1(a) was first

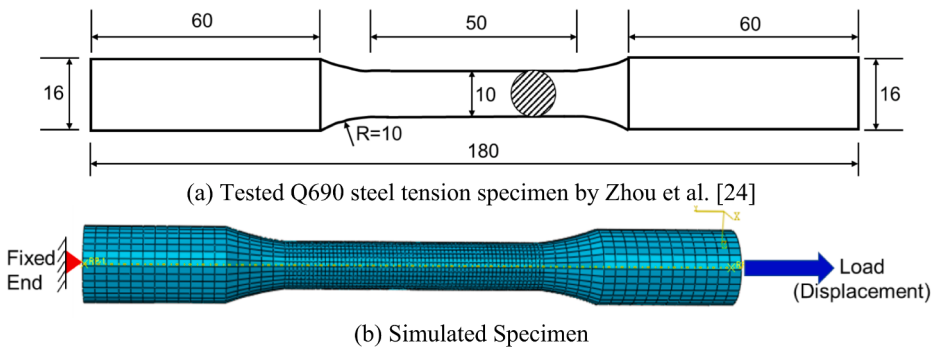


Fig. 1. Tested and simulated tension specimens made of Q690 steel.

heated in the electronic furnace to a given temperature within the range of 300 °C to 1000 °C, then the specimen was cooled by natural air or water, respectively. For a certain experienced temperature and cooling method, three similar specimens were tested to verify the accuracy of the test results [26].

The tested specimen was modeled in the finite element analysis program ABAQUS [42], as shown in Fig. 1(b). The three-dimensional solid brick element (C3D8R) was chosen to model the fracture behavior of the specimens, which works well for analyses with high material and geometric nonlinearity. To ensure the accuracy and convergence of the analysis, a mesh sensitivity study was conducted. Different mesh sizes ranging from 0.1 to 2 mm were used in the middle part of the tension specimen. To reduce the computational cost, relatively larger mesh size (e.g. 2–3 mm) was used in the simulated specimen where the stress concentration was less significant (e.g. near the ends of the simulated specimens). Since the analysis results can converge once the mesh size in the middle part of simulated specimen was no larger than 1 mm, a mesh size of 1 mm was finally used in the middle part of tension specimen and relatively coarse mesh (a mesh size within 2–3 mm) were employed near the ends of specimen. To simulate the boundary condition in the test, one end of the specimen was fixed in all degrees of freedom, while for the other end only the axial movement was allowed. The displacement-control method was used to load the specimen to fracture.

2.2. Determination of post-necking true stress-strain curves

For fracture analysis using finite element program, true stress-strain curves extending to a complete range which can describe the entire process of necking, fracture initiation and propagation are always needed. Prior to necking, true stress-strain relationships can be directly calibrated from Eqs. (1) and (2). After onset of necking, due to the complicated stress state and continuous reduction in the cross-sectional

area, it is difficult to obtain the post-necking true stress-strain curves from standard tensile tests. Therefore, a common approach to determining true stress-strain curves for ductile material after onset of necking is to input various true stress-true strain curves with different post-necking true stress-strain relationship in finite element analysis until the simulated engineering stress-strain curve matches well with the experimentally measured engineering stress-strain curve before fracture initiation point, as shown in Fig. 2. Using this approach, it was found that linear relationship between true stress and true strain can reasonably predict the measured engineering stress-strain curves.

$$\varepsilon_t = \ln(1 + \varepsilon_e) \quad (1)$$

$$\sigma_t = \sigma_e(1 + \varepsilon_e) \quad (2)$$

where σ_t , ε_t , σ_e and ε_e are the true stress, true strain, engineering stress and engineering strain, respectively.

The linear relationship between the true stress and strain after necking can be represented by the slope of the post-necking true stress-strain curves. Taking specimen shown in Fig. 2 as example, to determine the most suitable slope for post-necking true stress-strain curves, different slopes of the true stress-strain curves after necking were respectively input into the finite element model (e.g. 900 MPa, 830 MPa, 760 MPa and 690 MPa) to simulate the engineering stress-strain curve until the simulated result match best with the measured result before fracture. Fig. 3 illustrates the calibrated input true stress-strain curves for Q690 steel after being exposed to high temperatures for the air-cooling and water-cooling method, respectively. Tables 1 and 2 shows the calibrated slope of the post-necking true stress-strain curves using this approach for the two cooling methods, respectively. The ratio of slope under experienced temperature to initial slope without experiencing high temperature (slope ratio) was listed in the bracket in Tables 1 and 2. Generally, the slope of post-necking true stress-strain

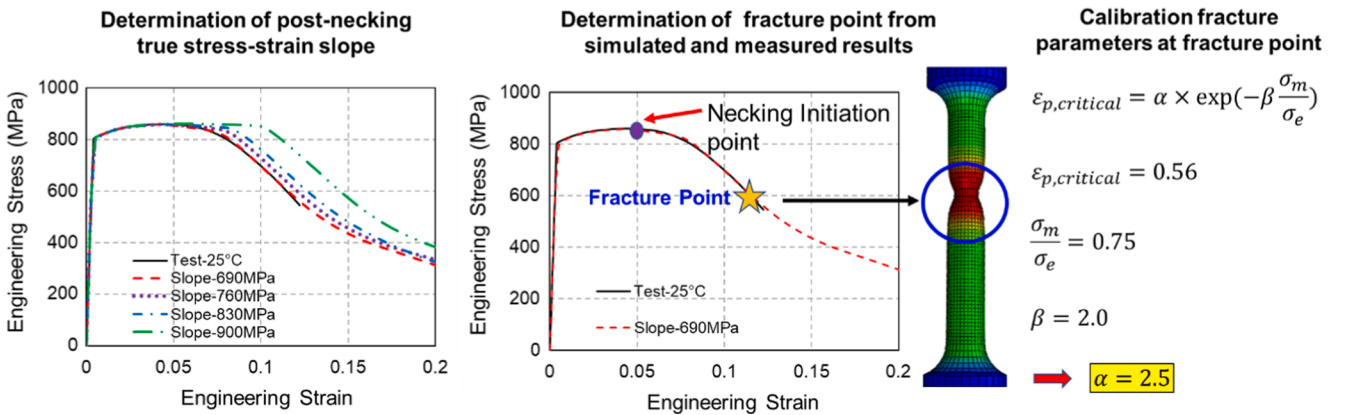


Fig. 2. Determination of post-necking true stress-strain curves and fracture model parameters.

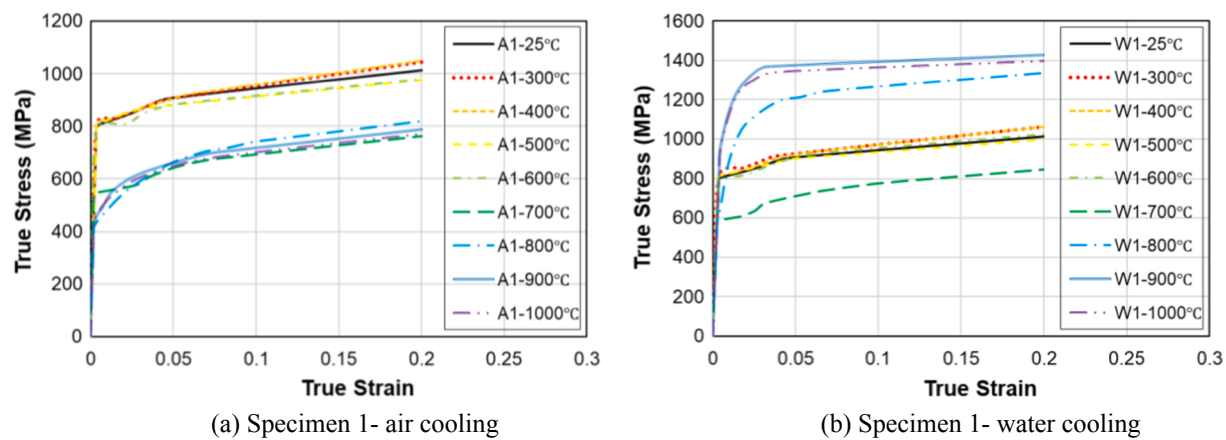


Fig. 3. Developed true stress-strain curves for Q690 steel after fire.

Table 1

Slope of post-necking true stress-strain curves for Q690 steel after fire with air-cooling method (MPa).

Temperature	25 °C	300 °C	400 °C	500 °C	600 °C	700 °C	800 °C	900 °C	1000 °C
A1-Slope	690 (1.0)	896 (1.3)	896 (1.3)	896 (1.3)	621 (0.9)	621 (0.9)	758 (1.1)	690 (1.0)	690 (1.0)
A2-Slope	690 (1.0)	690 (1.0)	690 (1.0)	621 (0.9)	621 (0.9)	690 (1.0)	621 (0.9)	690 (1.0)	758 (1.1)
A3-Slope	690 (1.0)	690 (1.0)	690 (1.0)	621 (0.9)	621 (0.9)	621 (0.9)	690 (1.0)	690 (1.0)	690 (1.0)
Average	690 (1.0)	758 (1.1)	758 (1.1)	712 (1.0)	621 (0.9)	644 (0.9)	690 (1.0)	690 (1.0)	712 (1.0)

Note: values in bracket are the ratio of slope after being exposed to given temperature to the initial slope at ambient temperature, which was 690 MPa.

Table 2

Slope of post-necking true stress-strain curves for Q690 steel after fire with water-cooling method (MPa).

Temperature	25 °C	300 °C	400 °C	500 °C	600 °C	700 °C	800 °C	900 °C	1000 °C
W1-Slope	690 (1.0)	896 (1.3)	896 (1.3)	621 (0.9)	690 (1.0)	621 (0.9)	690 (1.0)	345 (0.5)	345 (0.5)
W2-Slope	690 (1.0)	758 (1.1)	690 (1.0)	690 (1.0)	690 (1.0)	690 (1.0)	69 (0.1)	276 (0.4)	345 (0.5)
W3-Slope	690 (1.0)	758 (1.1)	690 (1.0)	207 (0.3)	690 (1.0)	758 (1.1)	690 (1.0)	345 (0.5)	345 (0.5)
Average	690 (1.0)	804 (1.2)	758 (1.1)	654 (0.9)	690 (1.0)	690 (1.0)	690 (1.0)	322 (0.5)	345 (0.5)

Note: values in bracket are the ratio of slope after being exposed to given temperature to the initial slope at ambient temperature, which was 690 MPa.

curves can somewhat represent the degree of softening of materials after necking. This is because that the larger the slope of post-necking true stress-strain curves, the more increase of true stress and the more reduction of cross-sectional area with the increase of true strain after necking would be. This can also lead to a larger degree of post-necking material softening. It was observed that for the air-cooling method, at given experienced temperature, the difference in the slope of the post-necking true stress-strain curves between three tested specimens with the same material properties are relatively small. However, the differences were more significant for water-cooling method, particularly for experienced temperatures of 500 °C and 800 °C. This indicates that the water-cooling method may result in a pronounced divergence of post-necking true stress-strain behavior for Q690 steel after being exposed to a high temperature (>500 °C). This may be because that water-cooling method can lead to a divergence of cooling rates and further result in a variety of material properties after cooling. Tables 1 and 2 also lists the average value of post-necking true stress-strain curves for three specimens under each experienced temperature. If the difference between one of the results and either of the other two results were beyond 30%, the result was excluded and only two similar results were averaged (e.g. 500 °C and 800 °C).

The results of Tables 1 and 2 were plotted as shown in Fig. 4. It clearly illustrates the variation trends of slope of post-necking true stress-strain curves with the maximum experienced temperatures. It can also demonstrate the critical experienced temperatures and cooling methods that result in a significant change of slopes of true stress-strain curves and the degree of material softening for Q690 steels. It was found

that the slope and slope ratio exhibited limited variations with the experienced temperatures for air-cooling condition. The maximum deviation was observed between 200 °C and 400 °C, which was an increase of approximately 30% in comparison to initial slope. For water-cooling condition, the maximum difference in slope from initial slope was nearly 90%. This indicate that water-cooling condition can lead to the various cooling rate level which may affect the post-necking material properties of Q690 steels significantly.

2.3. Determination of fracture model parameters

As one of representative fracture models, the accuracy of the stress modified critical strain (SMCS) model to predict fracture behavior of structural steels has been proved by several studies [5,43]. In SMCS model, only two material-dependent parameters need to be determined. Due to these advantages, SMCS became the commonly used fracture model and was added in the finite element computer program such as ABAQUS [42]. The SMCS model was chosen in this study to predict fracture behavior of high-strength steels after being exposed to high temperature. As shown in Eq. (3), in SMCS model, plastic strain at fracture initiation ($\epsilon_{p,\text{fracture}}$) is exponentially related to stress triaxiality (σ_m/σ_e). The fracture parameter α represents the toughness index as a measure of resistance to fracture initiation [5]. The larger the toughness index is, the stronger the fracture resistance of material is. The fracture parameter β is another material-dependent parameter, and it was generally within a small range (e.g. 1.5–2.3) for structural steels [35]. In this study, the fracture parameter β was assumed to be 2.0 and only the

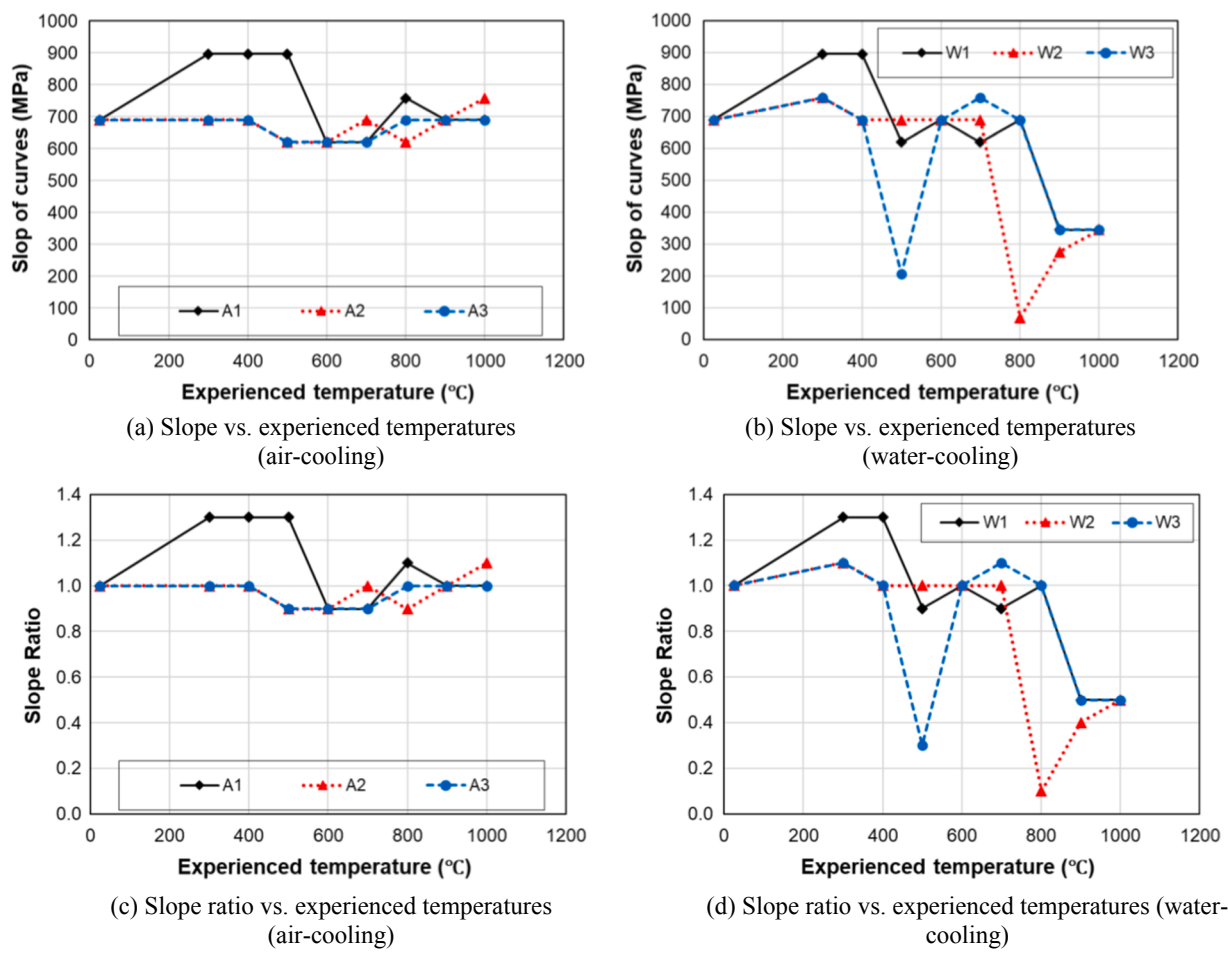


Fig. 4. Variation trends of slope of post-necking true stress-strain curves of Q690 steel after fire with experienced temperatures.

toughness index α was calibrated.

$$\varepsilon_{p,\text{fracture}} = \alpha \exp\left(-\beta \frac{\sigma_m}{\sigma_e}\right) \quad (3)$$

where $\varepsilon_{p,\text{fracture}}$ is the equivalent plastic strain; σ_m/σ_e is stress triaxiality; σ_m is the hydrostatic stress; σ_e is the von-Mises stress; α is the toughness index; β is the material-dependent parameters, $\beta = 2.0$.

The calibration of the toughness index α was based on experimental data and finite element analysis, as shown in Fig. 2. Firstly, the tested specimen as shown in Fig. 1 was modelled in ABAQUS without considering fracture behavior. The simulated engineering stress-strain curves was obtained and compared with measured results. Secondly, the fracture initiation point was then estimated from the measured engineering stress-strain curve, where the engineering stress started to reduce rapidly. Thirdly, the fracture initiation point determined from measured engineering stress-strain curve was tracked back to the simulated result and found out the corresponding finite element analysis step for this point. Finally, at the analysis step for the fracture initiation point, the stress triaxiality and plastic strain were output from simulated results.

Substitution of these two parameters into Eq. (3) yielded the toughness index α .

Using the above described procedure, the toughness index α for Q690 steel after being exposed to high temperature were obtained. Tables 3 and 4 list the toughness indices and toughness index ratios of three specimens after being exposed to different experienced temperatures based on air-cooling and water-cooling methods, respectively. The toughness index ratio was defined as the ratio of toughness index of steels after being exposed to a high temperature and cooling to initial toughness index before high-temperature exposure. This was listed in Tables 3 and 4 in bracket below the corresponding value of toughness index. For air-cooling method, a large difference ($>30\%$) of the toughness indices for three specimens was observed at experienced temperature of $300\text{ }^\circ\text{C}$. Therefore, for $300\text{ }^\circ\text{C}$, the toughness index of 0.5 of the first specimen was excluded when calibrating average value since it was much smaller than the toughness index of 2.0 for the other two specimens. For water-cooling method, this large difference in the toughness index was observed for more experienced temperature cases (e.g. $400\text{ }^\circ\text{C}$, $500\text{ }^\circ\text{C}$ and $800\text{ }^\circ\text{C}$). The average value of the toughness indices was

Table 3

Post-fire toughness index α of Q690 steel tension specimen cooled by air.

Temperature	$25\text{ }^\circ\text{C}$	$300\text{ }^\circ\text{C}$	$400\text{ }^\circ\text{C}$	$500\text{ }^\circ\text{C}$	$600\text{ }^\circ\text{C}$	$700\text{ }^\circ\text{C}$	$800\text{ }^\circ\text{C}$	$900\text{ }^\circ\text{C}$	$1000\text{ }^\circ\text{C}$
A1- α	2.5 (1.0)	0.5 (0.2)	1 (0.4)	2 (0.8)	2 (0.8)	2 (0.8)	2 (0.8)	1.5 (0.6)	2 (0.8)
A2- α	2.5 (1.0)	2 (0.8)	1.5 (0.6)	2 (0.8)	2 (0.8)	2 (0.8)	2 (0.8)	1.5 (0.6)	1.5 (0.6)
A3- α	2.5 (1.0)	2 (0.8)	2 (0.8)	2 (0.8)	2 (0.8)	2 (0.8)	2 (0.8)	1.5 (0.6)	1 (0.4)
Average	2.5 (1.0)	2 (0.8)	1.5 (0.6)	2 (0.8)	2 (0.8)	2 (0.8)	2 (0.8)	1.5 (0.6)	1.5 (0.4)

Note: values in bracket are the ratio of toughness index after being exposed to given temperature to the initial toughness index at ambient temperature, which was 2.5.

Table 4

Post-fire toughness index of Q690 steel tension specimen cooled by water.

Temperature	25 °C	300 °C	400 °C	500 °C	600 °C	700 °C	800 °C	900 °C	1000 °C
W1 - α	2.5 (1.0)	1.5 (0.6)	0.2 (0.1)	0.5 (0.2)	2 (0.8)	2 (0.8)	0.5 (0.2)	1.5 (0.6)	1.5 (0.6)
W2 - α	2.5 (1.0)	2 (0.8)	1.5 (0.6)	0.5 (0.2)	2 (0.8)	2 (0.8)	0.1 (0.04)	1.5 (0.6)	1.5 (0.6)
W3 - α	2.5 (1.0)	2.5 (1.0)	1.5 (0.6)	0.1 (0.04)	2 (0.8)	2 (0.8)	0.5 (0.2)	1.5 (0.6)	1.5 (0.6)
Average	2.5 (1.0)	2 (0.8)	1.5 (0.6)	0.5 (0.2)	2 (0.8)	2 (0.8)	0.5 (0.2)	1.5 (0.6)	1.5 (0.6)

Note: values in bracket are the ratio of toughness index after being exposed to given temperature to the initial toughness index at ambient temperature, which was 2.5.

calibrated using the similar approach to that for air-cooling method. The divergence of toughness index for the similar specimen (e.g. 300 °C for air-cooling method, 400 °C, 500 °C and 800 °C for water-cooling method) was caused by the discrepancy of the measured post-fire stress-strain behavior. For a given temperature and cooling method, the discrepancies may exist in heating and cooling rate during the test, resulting in a different microstructural change and further leading to quite different post-fire material properties. In addition, variability of materials may also affect their post-fire stress-strain behavior and fracture behavior. However, more tests with a large number of steel samples are still required to explore this discrepancy in the post-fire material behaviors of Q690 steels for a given exposure temperature and cooling method.

In order to obtain critical experienced temperature ranges for post-fire fracture resistance of Q690 steels and to generalize and propose reasonable toughness index for their post-fire fracture prediction, the variation trends of the toughness index and toughness index ratio with the experienced temperatures are illustrated in Fig. 5. As shown in Fig. 5 (a), when the specimen was cooled by air, for most of experienced

temperatures, toughness indices of the three specimens were close or exactly identical. In Fig. 5(b), the water-cooling method generated quite different toughness indices between the three specimens. The water-cooling method can even lead to the failure mode of Q690 steel tension specimen close to the brittle fracture after being experienced temperatures of 500 °C and 800 °C, because the toughness index was smaller than 0.5 for the given experienced temperatures. Fig. 5(c) and (d) illustrate the toughness index ratio for air-cooling method and water-cooling method, respectively. For both cooling methods, toughness index of Q690 steel reduced after being experienced high temperatures. In general, the water-cooling method resulted in a more degradation of toughness index than air-cooling method. The significant reduction (>60%) for the water-cooling condition was observed at experienced temperatures of 400 °C, 500 °C and 800 °C. The large reduction (>40%) observed for air-cooling condition was at experienced temperatures of 300 °C, 400 °C, 900 °C and 1000 °C. This indicates that the post-fire fracture resistance of Q690 steel tension specimen is sensitive to the cooling method and the experienced temperature.

Several factors may influence the post-fire toughness index of high-

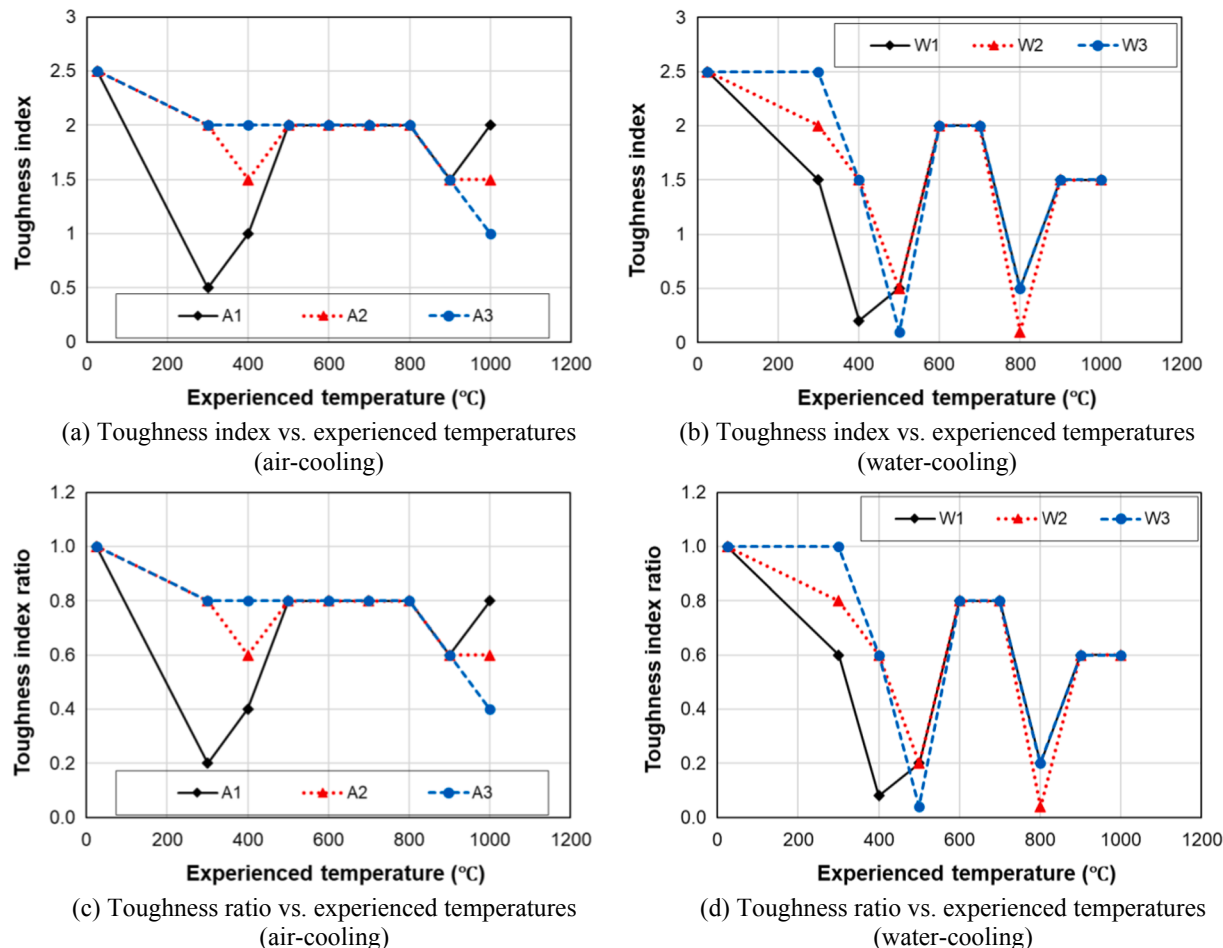


Fig. 5. Post-fire toughness index vs. experienced temperature curves for Q690 steel specimen.

strength steels, including chemical composition, grain size, and inclusions size. According to previous studies, higher temperature may enlarge the inclusions and austenite grain size, which results in the deterioration of the post-fire fracture resistance [44,45]. Large cooling rate may lead to the formation of hard and brittle composition such as martensite which reduces the post-fire fracture resistance of steels [3,4]. Therefore, after being experienced different temperatures and cooling methods, high-strength steels may undergo a variation of fracture resistance and toughness index. However, more metallurgical and microstructural analyses and a sufficient number of samples are still needed to establish the numerical relationship between the post-fire steel fracture resistance and experienced temperature and cooling rate.

2.4. Determination of damage evolution law

The development of damage evolution law was based on both true stress-strain curve and corresponding engineering stress-strain curve, as shown in Fig. 6. The damage of material is represented by the softening branch of engineering stress-strain curve, which is mainly due to the occurrence of necking, fracture initiation and fracture propagation. The development of damage in material can be quantitatively described using damage evolution law which is the function of damage index (D) and plastic displacement or deformation (U_{pl}), as shown in Eq. (4). The plastic displacement can be calibrated as the product of plastic strain (ϵ_{pl}) and characteristic length of element (L). In ABAQUS, the damage evolution law should be input into material properties to predict fracture behavior. It is input as a series of scattered data in terms of damage index (D) and plastic displacement or deformation (U_{pl}).

For a certain true stress, the damage index (D) can be calibrated using Eq. (4) when the corresponding engineering stress is determined. Note that the damage index is equal to zero at onset of necking and it is equal to 1.0 when the tension specimen is totally fractured. Using Eqs. (5) to (7), the corresponding plastic displacement for the true stress can be calibrated.

$$\sigma_e = (1 - D)\sigma_t \quad (4)$$

$$u_{pl} = \epsilon_{pl}L = [\epsilon_e - \frac{\sigma_e}{(1 - D)E} - \epsilon_{opl}]L \quad (5)$$

$$\epsilon_{opl} = \epsilon_n - \frac{\sigma_{max}}{E} \quad (6)$$

$$L = \sqrt[3]{abc} \quad (7)$$

where σ_e is the engineering stress, σ_t is the corresponding true stress, D is the damage index, u_{pl} is the plastic displacement, ϵ_{pi} is the plastic strain in the softening branch, ϵ_e is the engineering strain, ϵ_{opl} is the plastic strain at necking, E is the elastic modulus, L is the characteristic length of

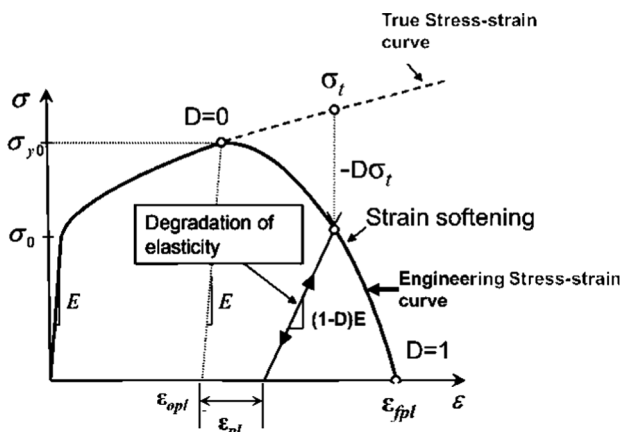


Fig. 6. Calibration of damage evolution law.

element which is the cubic root of the product of length (a), width (b) and depth (c) of element shown in Eq. (7), ϵ_n is the engineering strain at necking point, and σ_{max} is the maximum engineering stress which is also defined as the engineering stress at necking.

To establish the damage evolution law, different damage indices and corresponding plastic displacements should be calibrated. Using curve-fitting approach, it was found that the plastic displacement (U_{pl}) was exponentially related to the damage index (D), as expressed by Eq. (8). The values of the parameters u_0 and k in Eq. (8) at different experienced temperatures were determined by performing data fitting in software Origin. Tables 5 and 6 list the calibrated parameters u_0 and k for different Q690 steel tension specimens after being exposed to different temperatures based on air-cooling method and water-cooling method. According to Eq. (8), the greater the values of u_0 and k were, the larger the plastic displacement can be developed at a given damage index. Using Eq. (8) together with average parameters in Tables 5 and 6, the damage evolution law curves can be established in Fig. 7. The parameters were calibrated based on the element with a characteristic length of 1 mm.

$$u_{pl} = u_0 - u_0 \exp(-kD) \quad (8)$$

where u_0 and k are the damage parameters.

Fig. 7 demonstrates the damage evolution law curves of Q690 steel. It was found that the damage in Q690 steel developed more rapidly after being exposed to 400 °C and 800 °C and cooled by air. According to fracture toughness index in Section 2.3, the toughness indices of the specimen was smaller for 400 °C and 800 °C than that for the other temperature cases. This may be due to the rapid damage development in material at these two temperature cases. For water-cooling method, when the exposed temperatures are 500 °C and 800 °C, after the damage index approached to 0.2, no more plastic displacement developed in specimens and fracture occurred very rapidly. The rapid damage evolution resulted in a weak resistance to fracture in steel. According to Section 2.3. The toughness index for temperature cases of 500 °C and 800 °C was only 0.5 and the failure mode was even close to brittle fracture. Fig. 7 also presents the comparison of post-fire damage evolution curves between air-cooling and water-cooling method, respectively. The two cooling methods generated quite close damage evolution law curves with experienced temperature of 300 °C. For temperature cases of 400 °C, 600 °C and 700 °C, under the similar developed plastic displacement, the damage index was relatively smaller with water-cooling method than that with air-cooling condition. This indicates a slower damage development with water-cooling condition. However, for the experienced temperatures of 500 °C, 800 °C, 900 °C and 1000 °C, the opposite phenomenon was found. Therefore, the effect of cooling methods on damage evolution of Q690 steel varied with the experienced temperatures.

Damage evolution law is correlated to the stress state, ductility and fracture resistance. Therefore, the variation of damage evolution after high temperature exposure and cooling method may be affected by the factors including chemical composition, grain size, and inclusions size, which are similar to those for toughness index. To better explain the variation of post-fire damage evolution for high-strength steels after fire, more metallurgical and microstructural analyses are still needed.

2.5. Comparison of predicted and measured results

The average values of the post-necking material properties obtained from Sections 2.2 to 2.4 were used to numerically predict fracture behavior of Q690 steels. Fig. 8 illustrates the comparison of measured and predicted engineering stress-strain curves and fracture failure. The reasonable agreement between them demonstrates the accuracy of the calibrated true stress-strain curves, the fracture model and the damage evolution law. The plastic strain at fracture initiation were simulated with a reasonable accuracy since the maximum difference was

Table 5

Post-fire damage evolution law parameters of Q690 steel tension specimen cooled by air.

Damage parameter		Temperature								
		25 °C	300 °C	400 °C	500 °C	600 °C	700 °C	800 °C	900 °C	1000 °C
A1	u_0	0.13	0.07	0.05	0.09	0.12	0.13	0.07	0.11	0.11
	k	4.77	7.84	9.48	3.64	3.21	3.00	4.78	4.29	5.15
A2	u_0	0.13	0.11	0.04	0.09	0.12	0.13	0.06	0.10	0.13
	k	3.44	4.44	8.32	3.80	3.21	2.85	6.19	3.92	3.99
A3	u_0	0.13	0.09	0.10	0.09	0.12	0.14	0.09	0.12	0.14
	k	4.34	6.49	4.10	3.79	3.21	2.76	3.88	4.64	4.29
Average	u_0	0.13	0.09	0.06	0.09	0.12	0.13	0.07	0.11	0.13
	k	4.18	6.26	7.30	3.74	3.21	2.87	4.95	4.28	4.48

Table 6

Post-fire damage evolution law parameters of Q690 steel tension specimen cooled by water.

Damage parameter		Temperature								
		25 °C	300 °C	400 °C	500 °C	600 °C	700 °C	800 °C	900 °C	1000 °C
W1	u_0	0.13	0.09	0.03	0.04	0.14	0.13	0.02	0.07	0.07
	k	4.77	8.25	9.81	8.76	2.55	2.73	9.00	5.39	5.34
W2	u_0	0.13	0.06	0.07	0.04	0.13	0.13	0.03	0.09	0.08
	k	3.44	7.49	5.22	9.46	2.68	2.89	9.81	5.69	7.42
W3	u_0	0.13	0.12	0.11	0.01	0.12	0.16	0.05	0.06	0.07
	k	4.34	2.67	2.37	9.00	3.81	3.21	7.49	6.07	7.24
Average	u_0	0.13	0.09	0.07	0.03	0.13	0.14	0.03	0.07	0.07
	k	4.18	6.14	5.80	9.07	3.01	2.94	8.77	5.72	6.67

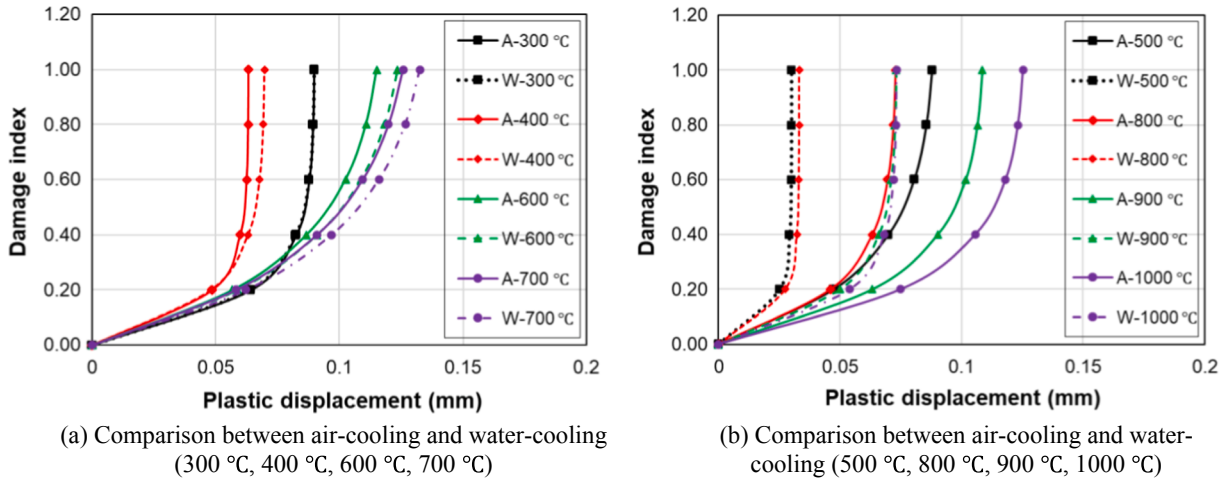


Fig. 7. Post-fire damage evolution law curves of Q690 steel tension specimen.

approximately 12% in comparison to the measured results.

3. Validation of post-fire fracture behavior for Q690 steels

Additional test results of Q690 steel tension specimens which were not used for calibration of post-necking material properties are required to further validate the calibrated material properties and fracture analysis approach for Q690 steel tension specimens. In this section, experimental results on post-fire mechanical properties of Q690 steels from Li et al. [27] and Wang and Lui [28] were used for validation of simulation models in previous section.

3.1. Test specimen and finite element model

The dimension of the tested specimens was shown in Fig. 9, which were designed based on GB/T228.1-2010 [41] and ASTM standard E8/E8M-16a [46], respectively. In the tests, both air-cooling and water-cooling methods were considered. For the natural air-cooling method,

the specimen was cooled naturally in the open furnace. For the water-cooling method, the specimen was immersed in the cold water after it was heated to the pre-selected temperature until its temperature decreased to the ambient temperature.

The numerical models of the specimens were created in ABAQUS [42]. The same element type (C3D8R), mesh size (minimum of 1 mm) and boundary condition similar to that in Section 2 were used. The true stress-strain curves, fracture model parameters and damage evolution law shown in Tables 1 to 6 were used to model post-necking material behavior of the specimens after fire.

3.2. Validation results

Figs. 10 and 11 shows the representative comparison of measured and predicted post-fire engineering stress-strain curves and failure mode for Q690 steel tension specimens for air-cooling and water-cooling method, respectively. The failure mode of the specimens from Wang and Lui [28] were not reported in the reference and only the predicted

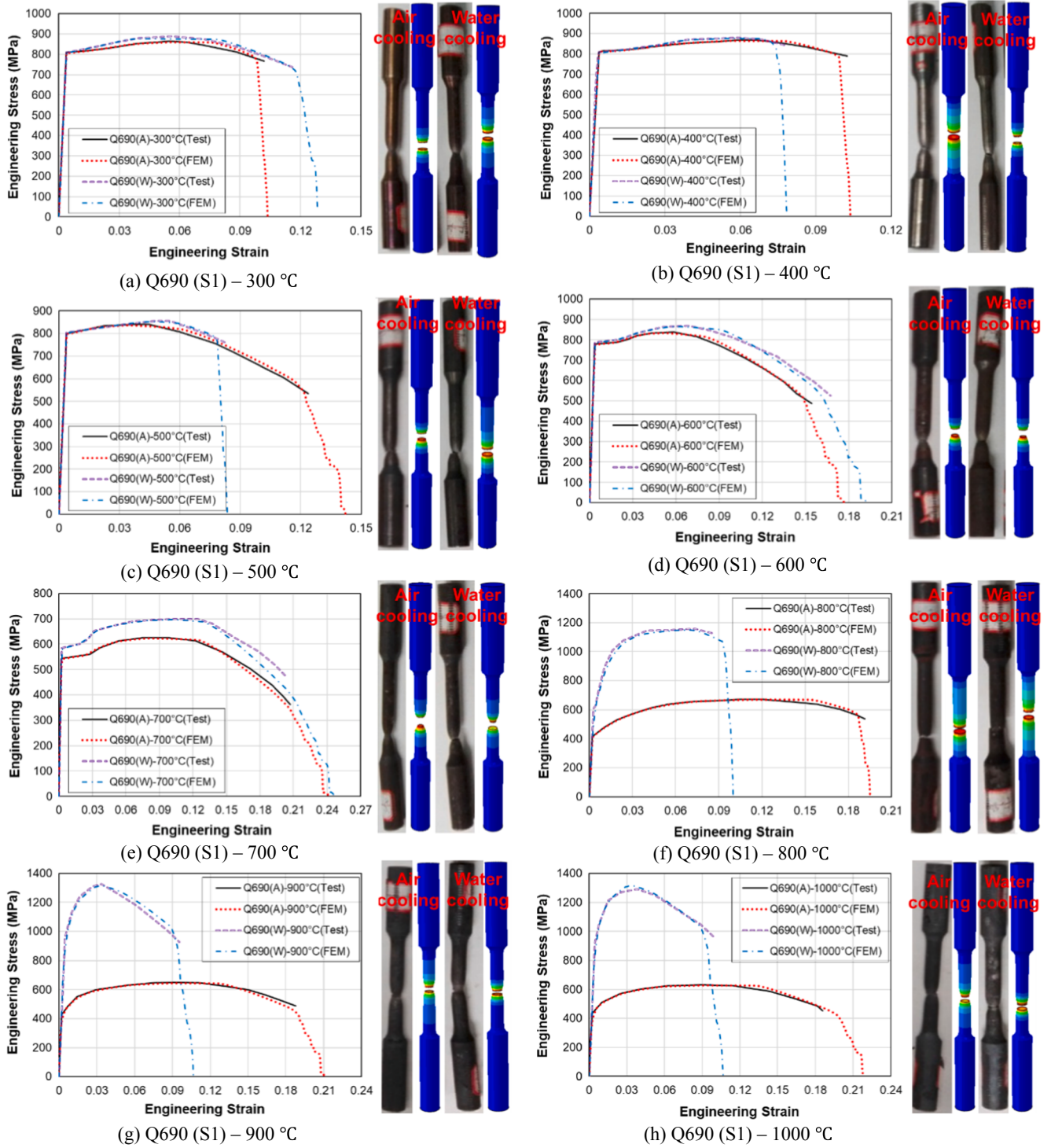


Fig. 8. Representative comparisons of test and simulation results for Q690 steel tension specimen after fire.

results were shown. For the air-cooling method as shown in Fig. 10, the simulation generally captured both engineering stress-strain behavior and failure modes with reasonably accuracy. The maximum difference in engineering strain at fracture initiation point between simulation and test was about 12% for the temperature of 800 °C and that in engineering stress at fracture initiation was within 10% for the temperature of 300 °C. The ductile fracture failure mode which is characterized by obvious reduction in cross-sectional area after fracture was observed in both tests and simulations. For the water-cooling method, a reasonable agreement was also achieved since the maximum difference in

engineering strain at fracture initiation was within 10% for the temperature of 500 °C and that in engineering stress at fracture initiation was within 5% for the temperature of 900 °C.

4. Post-fire fracture behavior of different high-strength steels

The validated approach in Sections 2 and 3 was used to investigate fracture behavior of other categories of high-strength steels in accordance with Chinese standard (type Q steels) and European standards (type S steels), including Q460, Q550, Q890, S460, S690, S960. The

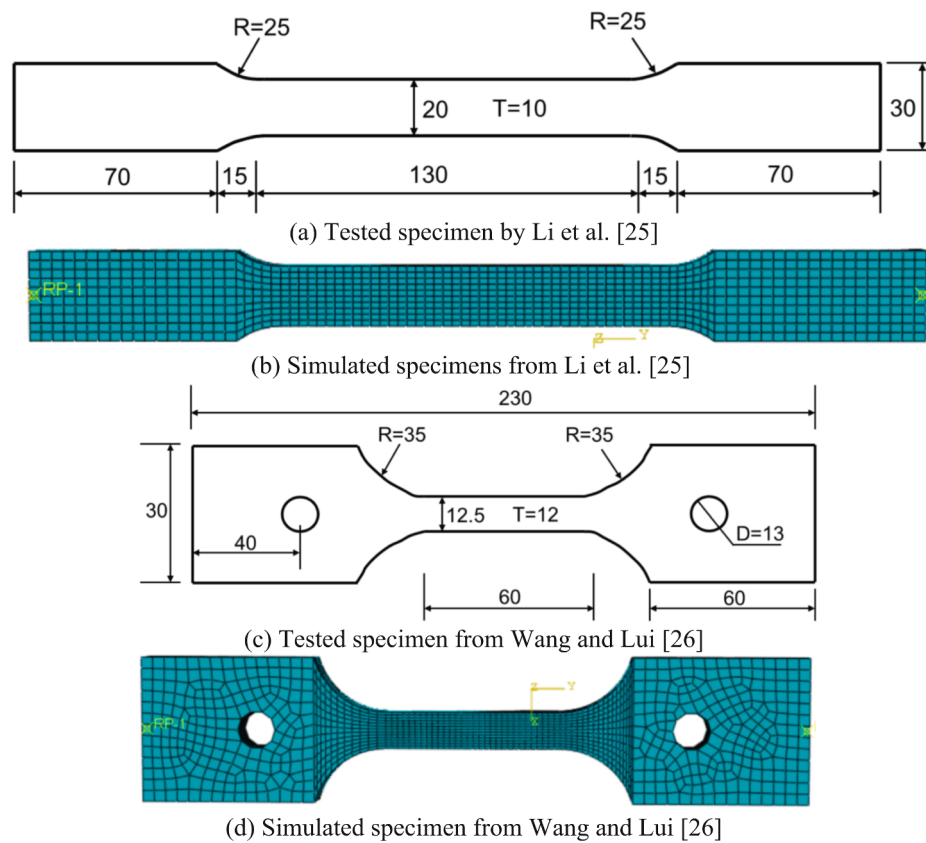


Fig. 9. Additional tested and simulated tension specimens made of Q690 steel (Unit: mm).

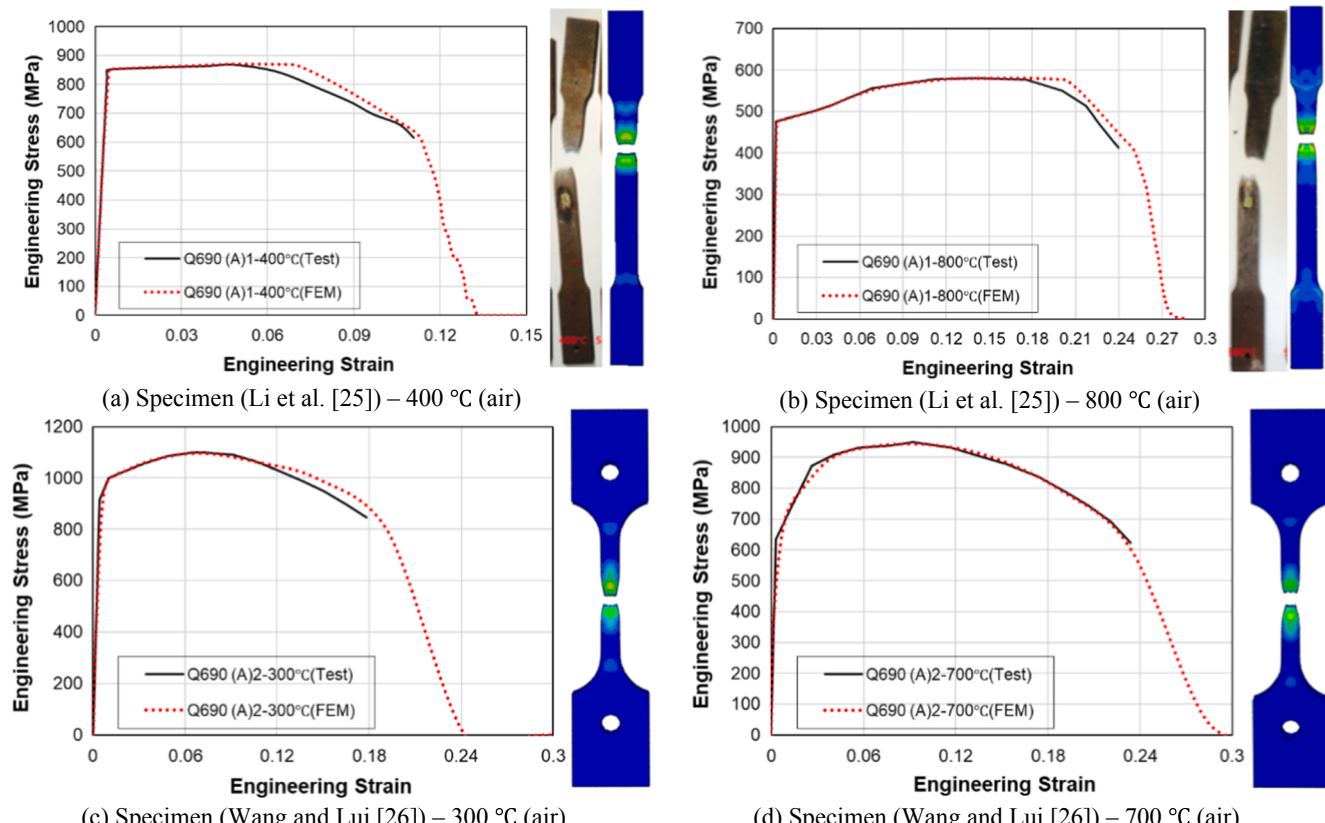


Fig. 10. Comparison of post-fire engineering stress-strain curves and failure mode of Q690 tensile specimen simulation based on air-cooling method.

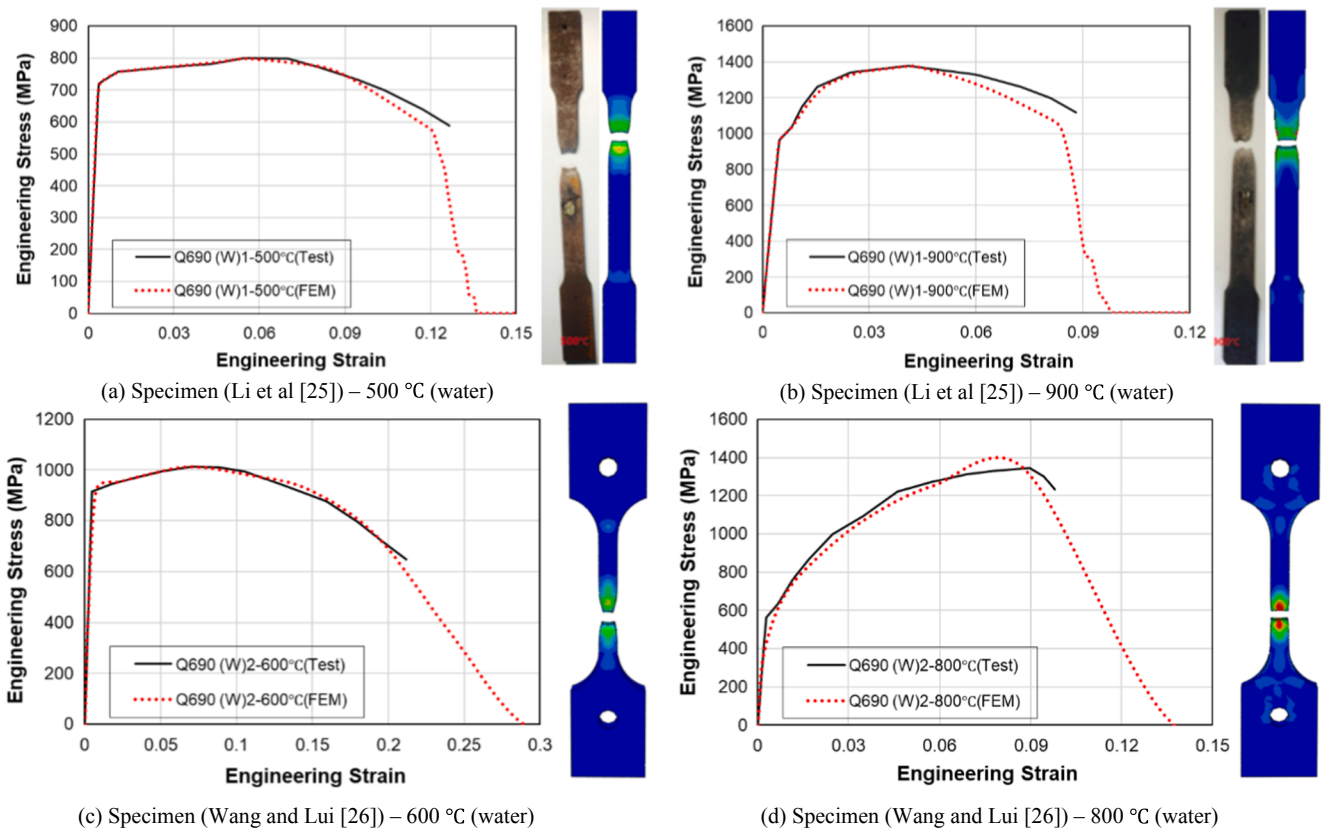


Fig. 11. Comparison of engineering stress-strain curves and failure mode of Q690 tensile specimen simulation based on water-cooling method.

post-necking true stress-strain curves, SMCS fracture model parameters and damage evolution laws for these tension specimens after fire were investigated. Note that due to lack of post-fire tensile test data considering water-cooling method for S460, S690, S960 steels, only the fracture behavior with air-cooling method of these steels were studied. The fracture behavior of the steels with same grades such as Q460 vs. S460 and Q690 vs. S690 were also compared.

4.1. Post-fire fracture behavior of Q460, Q550 and Q890 steels

The fracture behavior of Q460, Q550 and Q890 steels were investigated using both test data and numerical approach. They have a yield strength of 460 MPa, 550 MPa, 890 MPa, respectively. The dimension of Q460 specimens reported by Wang et al. [23] is shown in Fig. 12. (a), and that of Q550 specimens reported by Li et al. [47] and Q890

specimens reported by Lyu [48] was shown in Fig. 9 (a). They were designed based on Chinese standard [41]. The test procedure and method were similar to that for Q690 steel tension specimens described in Section 3.1. The numerical models of Q460, Q550 and Q890 tension specimens were created in ABAQUS [42], as shown in Fig. 12(b) and 9 (b), respectively. The selected type of element and the minimum mesh size were similar to Sections 2 and 3. The properties of post-necking true stress-strain curves, fracture model parameters and the damage evolution law were calibrated using the same procedure explained previously.

Tables 7 and 8 list the slopes together with slope ratios of post-necking true stress-strain curves of the high-strength steels after being exposed to the temperatures ranging from 200°C to 900 °C under air-cooling and water-cooling conditions, respectively. Fig. 13 shows the variation trends of slope ratios with experienced temperatures. For air-cooling, the slope of Q460-Q690 steels changed slightly (increase or decrease by 10%) after being exposed to high temperatures. The maximum increase in slope was 40% for Q890 steel after being exposed to 600 °C. For water-cooling, when being exposed to a temperature higher than 600 °C, the slopes of the steels demonstrated significant change (decrease or increase more than 40%). This indicates that high-temperature exposure (≥ 600 °C) and the water-cooling method may lead to a more significant change in post-necking true stress-strain behaviors of Q460-Q690 high-strength steels. These may be due to the significant change of steel composition, inclusions and grain size after being exposed to higher temperature and larger cooling rate [3,4,44,45].

Tables 9 and 10 list the calibrated toughness indices α in SMCS model together with toughness index ratio for Q460-Q890 steels for different experienced temperatures with air-cooling and water-cooling method, respectively. The parameter β in SMCS model was assumed to be 2.0. Fig. 14 depicts the variations of toughness index ratio with experienced temperatures. For air-cooling condition, after being exposed to a temperature ranging from 200 °C to 900 °C, all the steels exhibited a

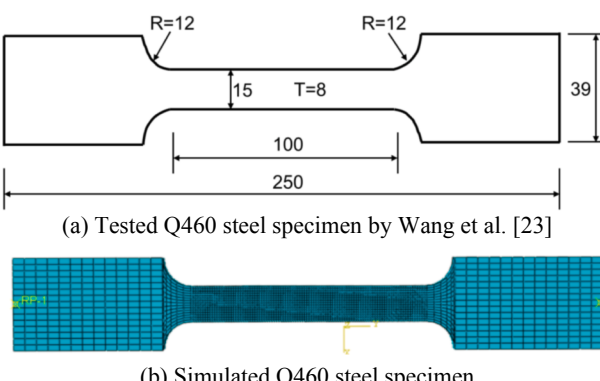


Fig. 12. Tested and simulated tension specimens made of Q460 steel by Wang et al. [23].

Table 7

Slope of post-necking true stress-strain curves of Q460-Q890 steels after high temperature with air-cooling method.

Temperature	25 °C	300 °C	400 °C	500 °C	600 °C	700 °C	800 °C	900 °C
Q460 (A) - Slope	690 (1.0)	690 (1.0)	690 (1.0)	690 (1.0)	690 (1.0)	690 (1.0)	690 (1.0)	690 (1.0)
Q550 (A) - Slope	690 (1.0)	758 (1.1)	758 (1.1)	690 (1.0)	690 (1.0)	690 (1.0)	690 (1.0)	690 (1.0)
Q690 (A) - Slope	690 (1.0)	758 (1.1)	758 (1.1)	712 (1.1)	621 (0.9)	644 (0.9)	690 (1.0)	690 (1.0)
Q890 (A) - Slope	690 (1.0)	896 (1.3)	827 (1.2)	827 (1.2)	965 (1.4)	690 (1.0)	896 (1.3)	690 (1.0)

Note: values in bracket are the ratio of slope after being exposed to given temperature to the initial slope at ambient temperature, which was 690 MPa.

Table 8

Slope of post-necking true stress-strain curves of Q460-Q890 steels after high temperature with water-cooling method.

Temperature	25 °C	300 °C	400 °C	500 °C	600 °C	700 °C	800 °C	900 °C
Q460 (W) - Slope	690 (1.0)	690 (1.0)	758 (1.1)	690 (1.0)	758 (1.1)	690 (1.0)	690 (1.0)	690 (1.0)
Q550 (W) - Slope	690 (1.0)	827 (1.2)	758 (1.1)	758 (1.1)	690 (1.0)	690 (1.0)	345 (0.5)	345 (0.5)
Q690 (W) - Slope	690 (1.0)	804 (1.2)	758 (1.1)	654 (0.9)	690 (1.0)	690 (1.0)	690 (1.0)	322 (0.5)
Q890 (W) - Slope	690 (1.0)	827 (1.2)	827 (1.2)	758 (1.1)	965 (1.4)	827 (1.2)	965 (1.4)	965 (1.4)

Note: values in bracket are the ratio of slope after being exposed to given temperature to the initial slope at ambient temperature, which was 690 MPa.

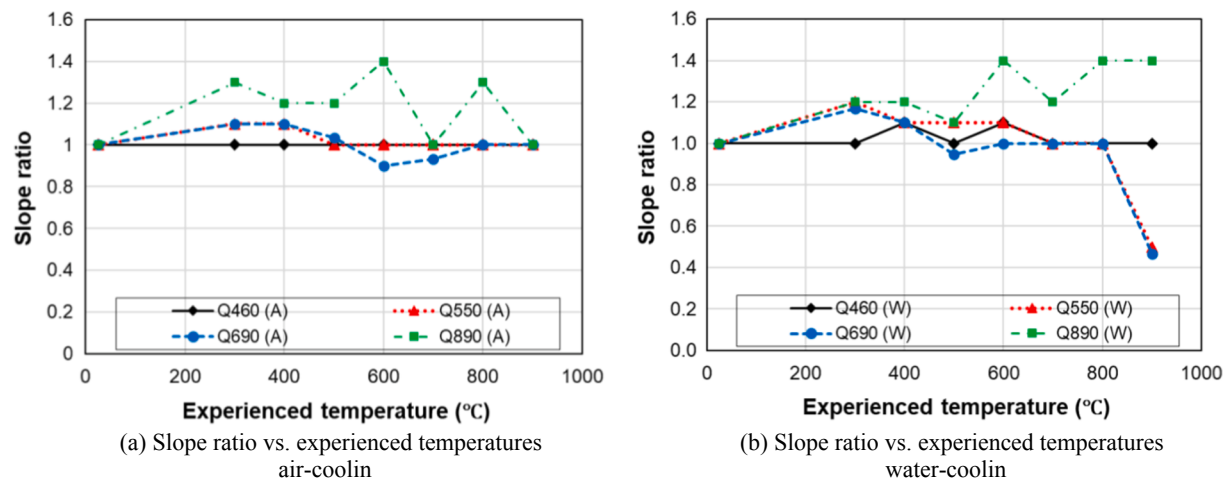


Fig. 13. Comparison of variations of slope ratios of post-necking true stress-strain curves of Q460-Q890 steels with experienced temperatures.

Table 9

Post-fire toughness index of Q460-Q890 steels with air-cooling method.

Temperature	25 °C	300 °C	400 °C	500 °C	600 °C	700 °C	800 °C	900 °C
Q460 (A) - α	2.5 (1.0)	2.0 (0.8)	2.0 (0.8)	2.0 (0.8)	2.0 (0.8)	2.0 (0.8)	1.0 (0.4)	2.0 (0.8)
Q550 (A) - α	2.5 (1.0)	2.0 (0.8)	2.0 (0.8)	2.0 (0.8)	2.0 (0.8)	2.0 (0.8)	2.0 (0.8)	2.0 (0.8)
Q690 (A) - α	2.5 (1.0)	2.0 (0.8)	1.5 (0.6)	2.0 (0.8)	2.0 (0.8)	2.0 (0.8)	2.0 (0.8)	1.5 (0.6)
Q890 (A) - α	2.5 (1.0)	1.5 (0.6)	1.5 (0.6)	2.0 (0.8)	2.0 (0.8)	2.0 (0.8)	1.5 (0.6)	1.5 (0.6)

Note: values in bracket are the ratio of toughness index after being exposed to given temperature to the initial toughness index at ambient temperature, which was 2.5.

Table 10

Post-fire toughness index of Q460-Q890 steels with water-cooling method.

Temperature	25 °C	300 °C	400 °C	500 °C	600 °C	700 °C	800 °C	900 °C
Q460 (W) - α	2.5 (1.0)	2.0 (0.8)	2.0 (0.8)	2.0 (0.8)	2.0 (0.8)	2.0 (0.8)	1.0 (0.4)	1.5 (0.6)
Q550 (W) - α	2.5 (1.0)	2.0 (0.8)	2.0 (0.8)	2.0 (0.8)	2.0 (0.8)	2.0 (0.8)	1.0 (0.4)	1.5 (0.6)
Q690 (W) - α	2.5 (1.0)	2.0 (0.8)	1.5 (0.6)	0.5 (0.2)	2.0 (0.8)	2.0 (0.8)	0.5 (0.2)	1.5 (0.6)
Q890 (W) - α	2.5 (1.0)	2.5 (1.0)	1.5 (0.6)	2.0 (0.8)	1.5 (0.6)	2.0 (0.8)	1.0 (0.4)	1.5 (0.6)

Note: values in bracket are the ratio of toughness index after being exposed to given temperature to the initial toughness index at ambient temperature, which was 2.5.

reduction in toughness index which indicated that the fracture resistance of Q460-Q890 steel tension specimens reduced after fire. For air-cooling condition, 400 °C and 800 °C were the most critical temperatures because most of the steels exhibited maximum reduction after being exposed to these temperatures. Under water-cooling condition,

Q690 steels demonstrated most degree of reduction in toughness index after being exposed to temperatures of 500 °C and 800 °C and the residual toughness index was only 20%.

Tables 11 and 12 list the calibrated parameters (u_0 and k) in damage evolution law shown in Eq. (8) for Q460-Q890 steels after being exposed

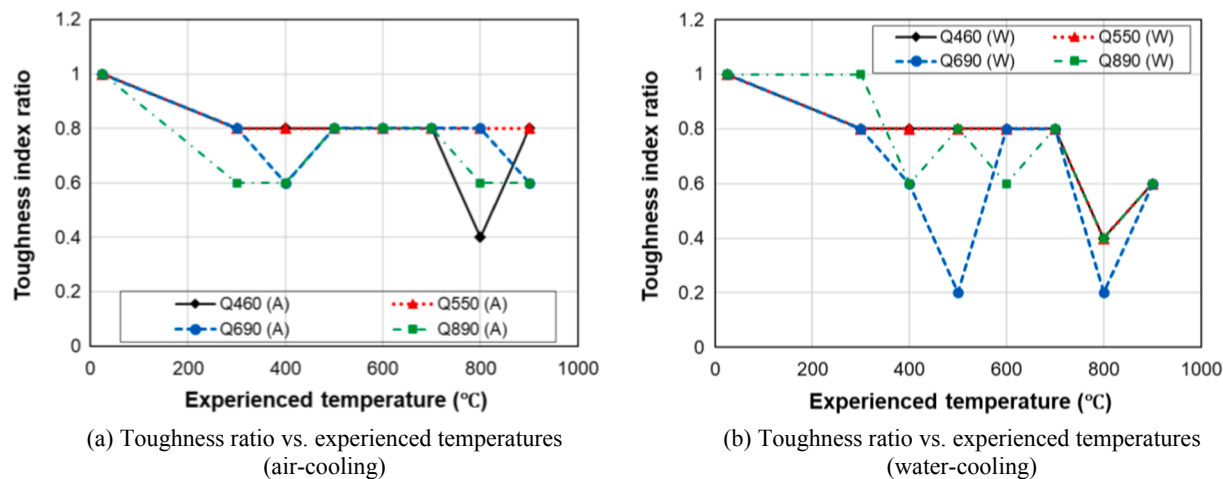


Fig. 14. Comparison of variation of toughness index of Q460-Q890 steels with experienced temperatures.

Table 11

Post-fire damage evolution law parameters of Q460-Q890 steels with air-cooling method.

Damage parameter		Temperature								
		25 °C	300 °C	400 °C	500 °C	600 °C	700 °C	800 °C	900 °C	1000 °C
Q460 (A)	u_o	0.10	0.09	0.09	0.10	0.09	0.10	0.07	0.08	0.10
	k	4.74	4.54	3.63	3.67	5.88	3.03	5.39	3.64	4.74
Q550 (A)	u_o	0.10	0.10	0.10	0.10	0.10	0.10	0.10	0.10	0.10
	k	5.67	3.45	4.71	4.1	3.54	4.78	3.23	3.5	5.67
Q690 (A)	u_o	0.13	0.09	0.06	0.09	0.12	0.13	0.07	0.11	0.13
	k	4.18	6.26	7.30	3.74	3.21	2.87	4.95	4.28	4.48
Q890 (A)	u_o	0.10	0.07	0.07	0.08	0.08	0.08	0.07	0.07	0.10
	k	5.59	8.69	6.89	5.75	5.47	6.52	5.38	7.17	5.59

Table 12

Post-fire damage evolution law parameters of Q460-Q890 steels with water-cooling method.

Damage parameter		Temperature								
		25 °C	300 °C	400 °C	500 °C	600 °C	700 °C	800 °C	900 °C	1000 °C
Q460 (W)	u_o	0.10	0.10	0.10	0.09	0.10	0.09	0.11	0.11	0.10
	k	4.74	4.90	4.21	4.70	3.82	4.94	2.65	2.64	4.90
Q550 (W)	u_o	0.10	0.08	0.10	0.09	0.09	0.10	0.06	0.06	0.08
	k	5.67	3.63	4.37	4.16	5.11	4.08	7.38	5.98	3.63
Q690 (W)	u_o	0.13	0.09	0.07	0.03	0.13	0.14	0.07	0.07	0.09
	k	4.18	6.14	5.8	9.07	3.01	2.94	8.77	5.72	6.14
Q890 (W)	u_o	0.10	0.08	0.07	0.07	0.08	0.10	0.05	0.07	0.08
	k	5.59	5.94	6.96	6.73	5.47	4.59	7.33	9.32	5.94

to different temperatures with air-cooling and water-cooling method, respectively. Using these parameters together with Eq. (8), the representative damage evolution law curves of Q460-Q890 steel tension specimens after being exposed to different temperature were established as shown in Fig. 15. For air-cooling condition, at a certain plastic displacement, the damage index was larger under the experienced temperature of 800 °C than that under other experienced temperatures, indicating a more rapid damage development in steels after being exposed to 800 °C. For water-cooling condition, all the steels also demonstrated rapid development of damage after being exposed to 800 °C, which was characterized by a sharp increase in damage index from 0.2 to 1.0 after the plastic displacement reaching to a certain level.

Fig. 16 illustrates a comparison of measured and predicted engineering stress-strain curves and fracture failure modes of Q460-Q890 steels after being exposed to different temperatures with air-cooling and water-cooling conditions. The comparison shows that the calibrated post-necking material properties can accurately simulate the whole process of necking and fracture for Q460-Q890 steels. The

maximum deviation in the predicted fracture initiation strain was approximately within 16%. Therefore, these derived parameters can be used as reference for predicting the post-fire fracture behavior of Q460-Q890 steels.

4.2. Post-fire fracture behavior of S460, S690 and S960 steels

The post-fire fracture behaviors of high-strength steel S460, S690 and S960, which have minimum specified yield strengths of 460 MPa, 690 MPa and 960 MPa, respectively, were investigated herein. Only air-cooling condition was considered due to lack of test data related to water-cooling condition. The test results reported by Qiang et al. [16,17] and finite element analysis were used to calibrate the post-necking material parameters for these steels after being exposed to high temperatures. The dimension of the tested S460-S960 steel tension from tests [16,17] and the numerical model of the specimens were shown in Fig. 17 (a) and Fig. 17(b), respectively. The modeling approach, type of element, mesh size and boundary condition were similar to those in

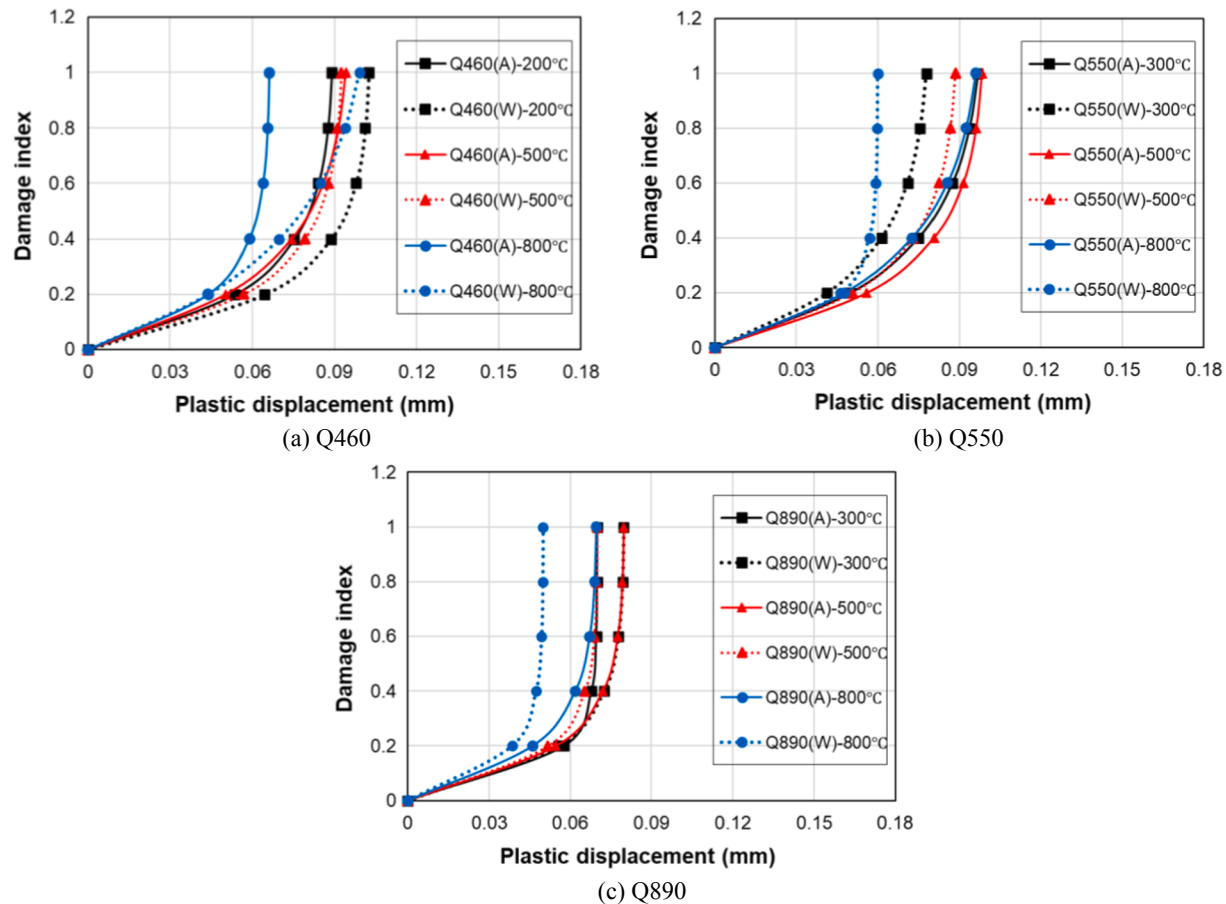


Fig. 15. Post-fire damage evolution law curves of Q460-Q890 steels.

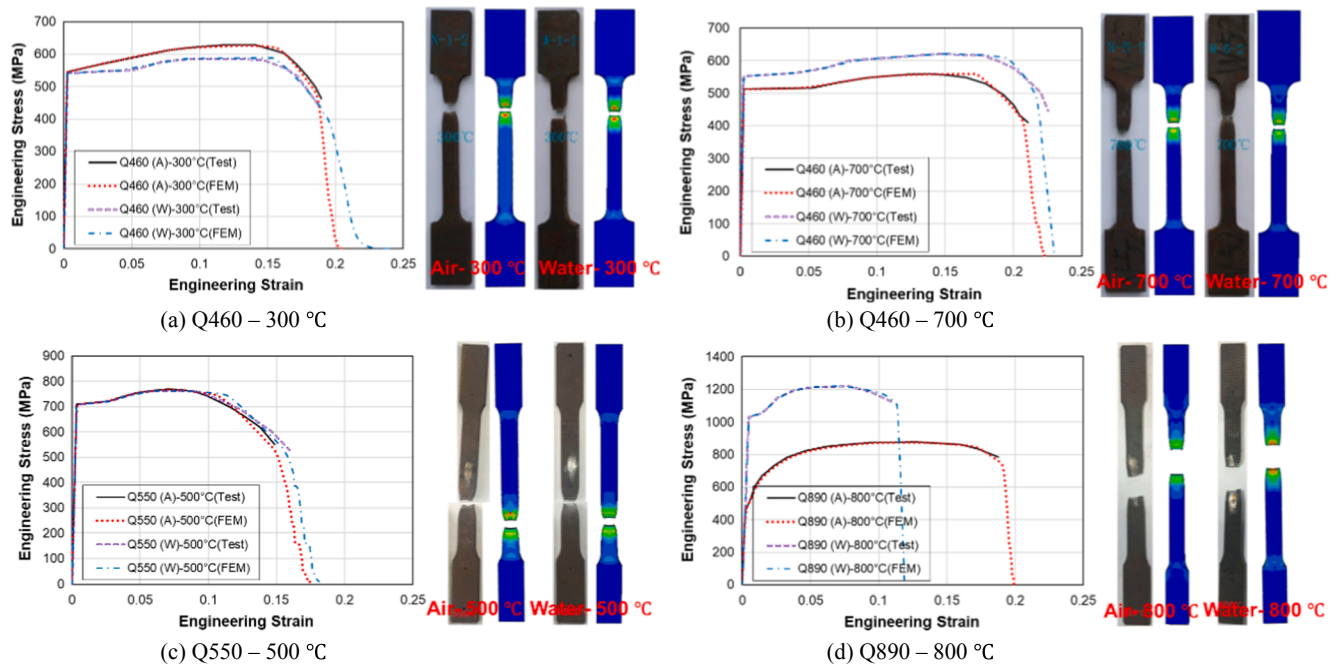


Fig. 16. Representative comparison of engineering stress-strain curves of Q460-Q890 steels after being exposed to high temperatures.

Section 4.1.

Table 13 lists the slope and ratio (value in bracket) of post-necking true stress-strain curves for S460-S960 steels. Fig. 18 depicts the

variation trends of slope and slope ratio with the experienced temperatures. It was found that between 600 °C and 750 °C, all the steels exhibited a reduction (<60%) in slope of post-necking true stress-strain

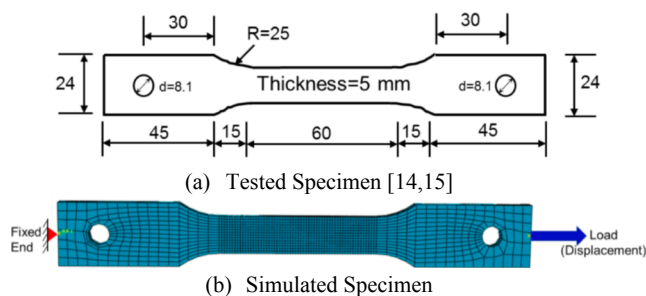


Fig. 17. Tested and simulated tension specimens made of S460-S960 steel by Qiang et al. [14,15].

curves. Beyond 750 °C, S690 and S960 steels demonstrated a significant increase in slope (>50%). This indicates the high experienced temperatures (>600 °C) may significantly affect the softening of S690 and S960 steels after onset of necking.

Table 14 lists the toughness indices for different steels. Ratio of toughness index after being exposed to high temperatures to initial toughness index was also calculated for comparison. Fig. 19 illustrates the variation of toughness index with experienced temperatures. Except for S960 steel, S460 and S690 steels only exhibited a reduction in toughness index after being exposed to a temperature higher than 600 °C. The maximum reduction was 75% which was observed for S960 steel after being experienced temperature of 850 °C. In general, after being exposed to high temperature (>600 °C), the fracture resistance of S460-

S960 reduced significantly.

The parameters of damage evolution law were determined using Eqs (4)–(7) and listed in Table 15. The representative damage evolution curves of S460, S690 and S960 were presented in Fig. 20. It was found that the critical experienced temperatures for S460, S690 and S960 was 750 °C, 650 °C and 850 °C, respectively. This is because the damage index increased more rapidly with the increase of plastic displacement for these temperatures than those for other experienced temperatures. Due to the rapid evolution of damage, the fracture resistance was relatively weaker for steels tension specimens after being exposed to these critical temperatures.

Using the post-necking material properties shown in Figs. 17 to 19, the engineering stress-strain curves and fracture failure mode were predicted in Fig. 21. The predicted engineering stress-strain curves were in a reasonable agreement with measured results. The differences between the measured and simulated results were within 12%. The failure mechanism captured by simulations matched well with measured failure mode. Therefore, the previously derived post-necking material properties can accurately predict post-fire fracture behavior of S460-S960 steels.

4.3. Comparison of post-fire fracture behavior of different high-strength steels

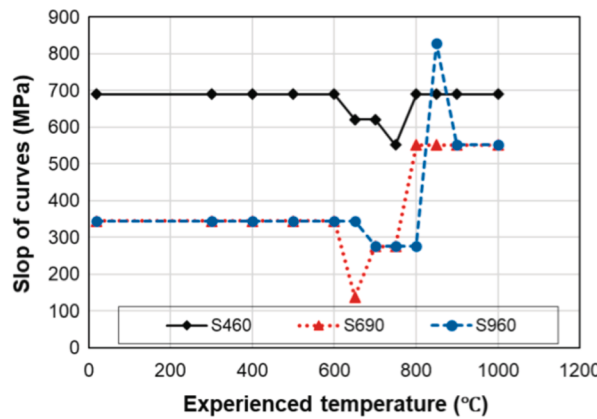
The slope of post-necking true stress-strain curves, toughness index in SMCS model and damage evolution laws for different types of high-strength steels with the same yield strength were compared as shown

Table 13

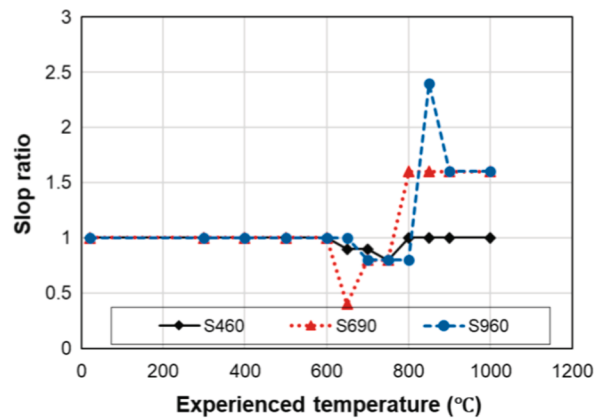
Slope of post-necking true stress-strain curves of S460-S960 steels after high temperature.

Temperature (°C)	20	300	400	500	600	650	700	750	800	850	900	1000
S460 - Slope	690 (1.0)	690 (1.0)	690 (1.0)	690 (1.0)	690 (1.0)	621 (0.9)	621 (0.9)	552 (0.8)	690 (1.0)	690 (1.0)	690 (1.0)	690 (1.0)
S690 - Slope	345 (1.0)	345 (1.0)	345 (1.0)	345 (1.0)	345 (1.0)	138 (0.4)	276 (0.8)	276 (0.8)	552 (1.6)	552 (1.6)	552 (1.6)	552 (1.6)
S960 - Slope	345 (1.0)	345 (1.0)	345 (1.0)	345 (1.0)	345 (1.0)	345 (0.1)	276 (0.8)	276 (0.8)	827 (2.4)	552 (1.6)	552 (1.6)	552 (1.6)

Note: values in bracket are the ratio of slope after being exposed to given temperature to the initial slope at ambient temperature, which were 690 MPa for S460 steel and 345 for S690 and S960 steels.



(a) Slope vs. experienced temperatures



(b) Slope ratio vs. experienced temperatures

Fig. 18. Comparison of variation of slope and slope ratio of post-necking true stress-strain curves of S460-S960 steels with experienced temperatures.

Table 14

Toughness index of S460-S960 steels after high temperature.

Temperature (°C)	20	300	400	500	600	650	700	750	800	850	900	1000
S460 - α	2.0 (1.0)	2.0 (1.0)	2.0 (1.0)	2.0 (1.0)	2.0 (1.0)	1.5 (0.75)	1.5 (0.75)	1.0 (0.5)	1.5 (0.75)	1.5 (0.75)	1.5 (0.75)	1.5 (0.75)
S690 - α	2.0 (1.0)	2.0 (1.0)	2.0 (1.0)	2.0 (1.0)	2.0 (1.0)	1.5 (0.75)	1.5 (0.75)	2.0 (1.0)	2.0 (1.0)	2.0 (1.0)	1.5 (0.75)	1.5 (0.75)
S960 - α	2.0 (1.0)	1.5 (0.75)	2.0 (1.0)	2.0 (1.0)	2.0 (1.0)	1.5 (0.75)	1.5 (0.75)	1.5 (0.75)	1.0 (0.5)	0.5 (0.25)	1.5 (0.75)	1.0 (0.5)

Note: values in bracket are the ratio of toughness index after being exposed to given temperature to the initial toughness index at ambient temperature, which was 2.0.

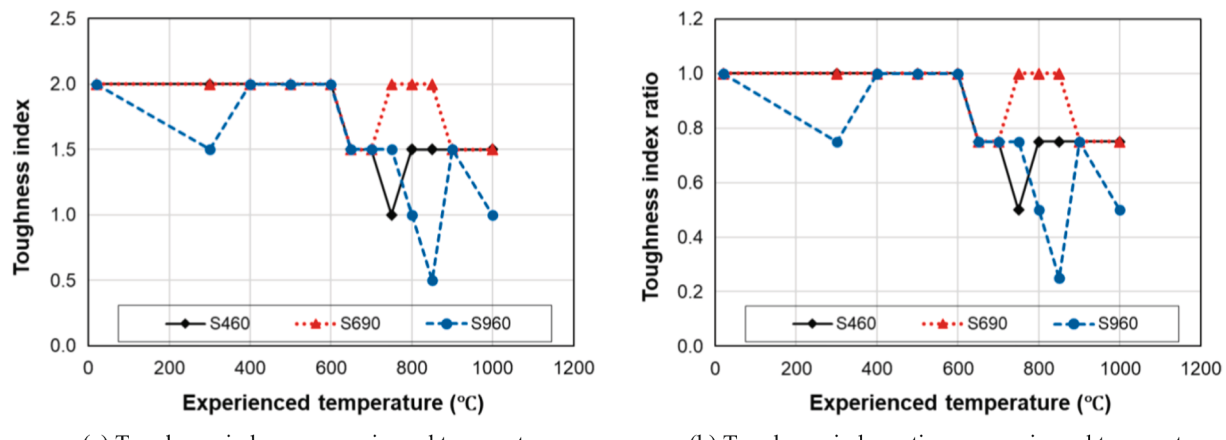


Fig. 19. Comparison of variations of toughness index and toughness index ratio of S460-S960 steels with experienced temperatures.

Table 15
Post-fire damage evolution law parameters of S460-S960 steels.

Damage parameter	Temperature (°C)												
	20	300	400	500	600	650	700	750	800	850	900	1000	
S460	u_o	0.08	0.08	0.08	0.09	0.08	0.09	0.09	0.07	0.1	0.09	0.08	0.08
	k	4.67	4.67	4.67	3.99	7.52	6.17	6.17	4.95	4.68	4.43	4.46	5.62
S690	u_o	0.07	0.07	0.07	0.07	0.06	0.04	0.06	0.07	0.1	0.09	0.06	0.06
	k	4.55	4.55	4.55	4.55	5.54	7.23	4.84	6.38	4.15	4.77	3.5	3.89
S890	u_o	0.06	0.05	0.06	0.06	0.06	0.06	0.05	0.06	0.04	0.04	0.05	0.04
	k	7.89	6.28	7.89	5.64	7.89	5.64	6.78	5.64	8.00	6.00	10.89	7.52

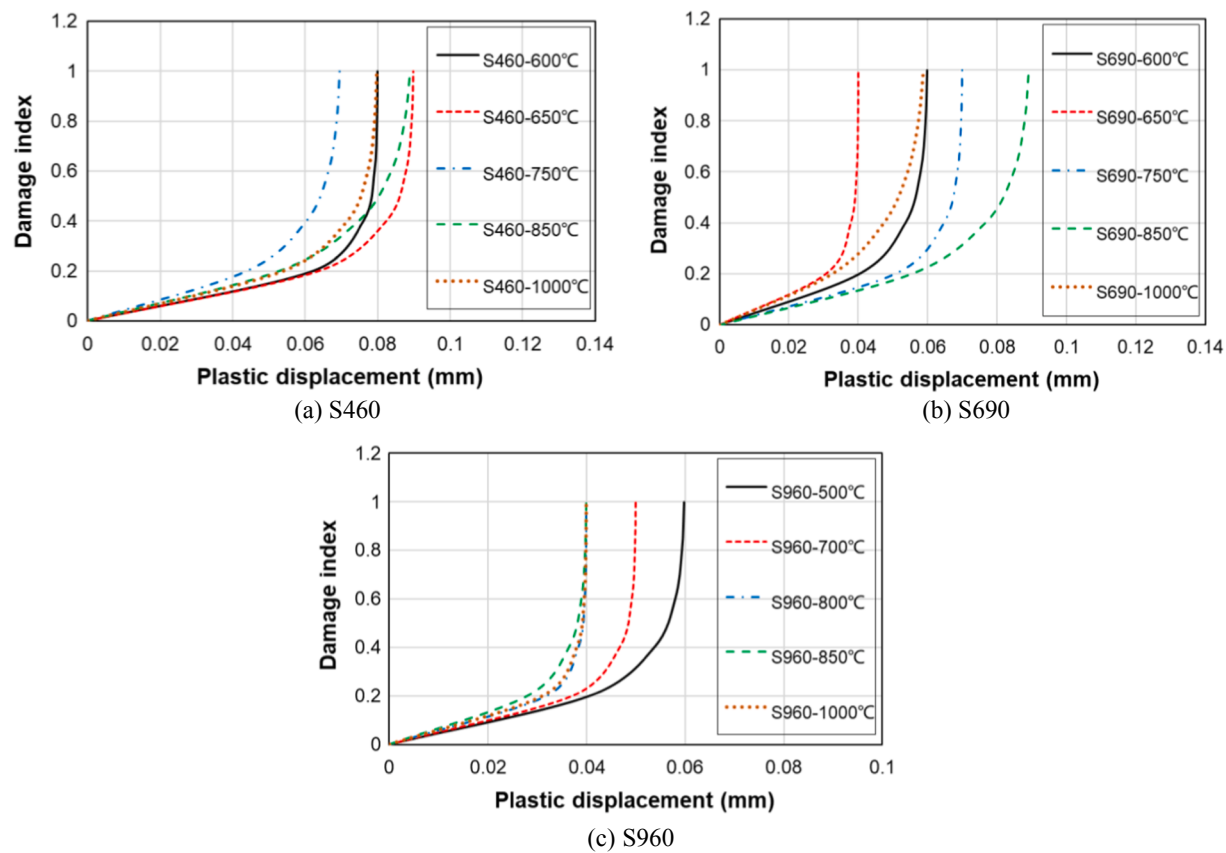


Fig. 20. Post-fire damage evolution law curves of S460-S960 steels.

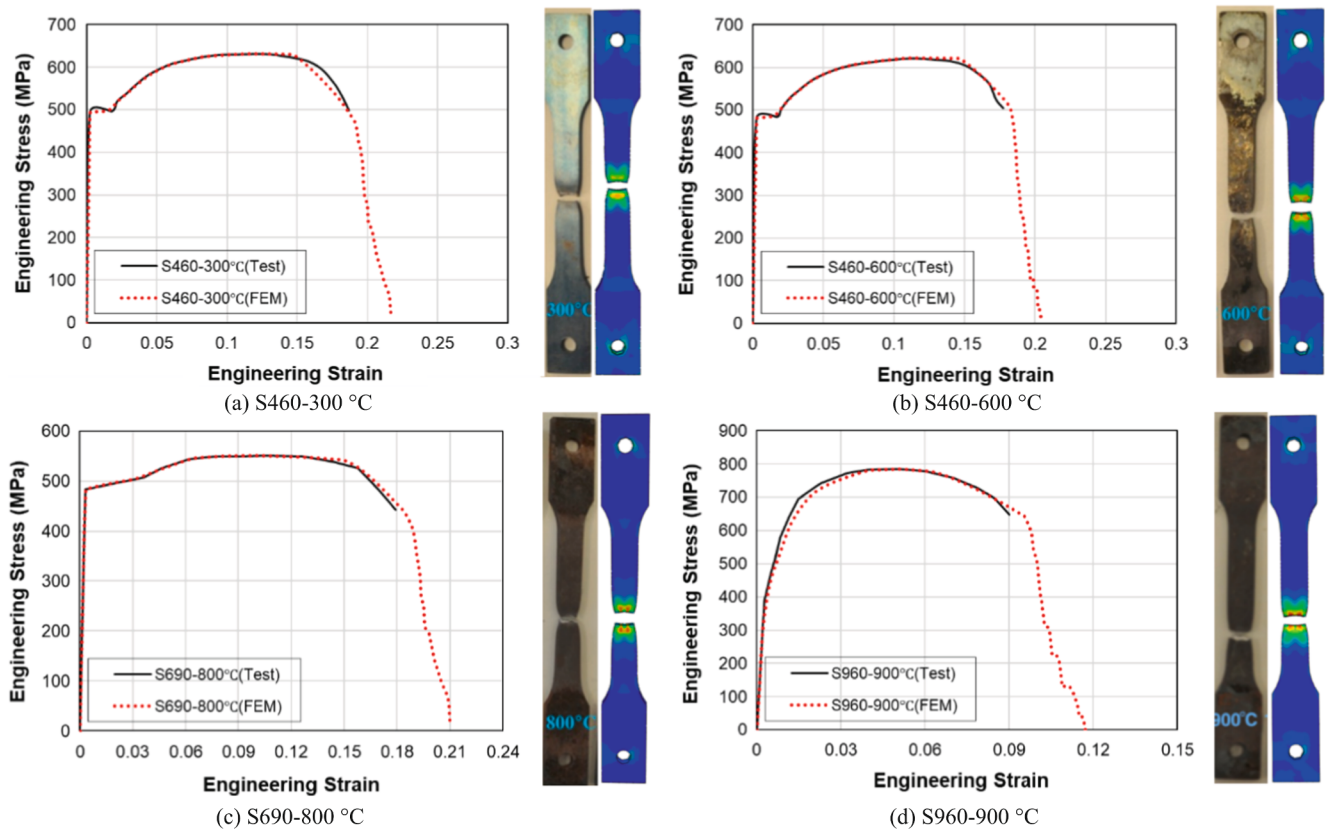


Fig. 21. Representative comparison of engineering stress-strain curves of S460-S960 steels after being exposed to high temperatures.

in Fig. 22. The slope of post-necking true stress-strain curves may affect the degree of strain softening. The toughness index in SMCS model is an index for fracture resistance of materials. Large toughness index indicates a higher resistance to fracture. The damage evolution law quantitatively describes the development of damage in material caused by necking and fracture. It is a function of damage index and plastic displacement. Damage initiates when necking occurs, and when damage index reached up to 1.0, materials completely fail. More rapid development of damage can lead to a lower resistance to fracture and less plastic deformation.

Fig. 22(a) compares the ratio of slope of post-necking true stress-strain curves of Q460, S460, Q690 and S690 steels after being exposed to high temperatures to initial slope. It was found that the slope ratio of post-necking true stress-strain curves of Q460 and S460 steels was practically invariant indicating that exposure to fire for 460 steels may not affect their softening after necking. For Q690 steels, the variation of post-necking slope was limited and within 20% after high temperature exposure. However, for S690 steel, once the exposure temperature was more than 700 °C, the post-necking slope even increased by 60%. This significant increase in post-necking slope is indicative of the considerable degree of softening of S690 steel after necking. Even for the same grade steels, they may still demonstrate quite different degree of post-necking softening after very high temperature exposure. High temperature may lead to a very complicated phase transformation process in steels, which results in a wide variety of steel compositions and material properties after cooling.

Fig. 22(b) depicts the variation of toughness index ratio of Q460, S460, Q690 and S690 steels after being exposed to high temperatures. For S-type steels, the toughness index decreased only when the experienced temperature was higher than 600 °C. The Q-type steels demonstrated quite different variation trends of toughness ratio with experienced temperatures. The maximum difference in toughness index ratio between Q460 steel and S460 steel was approximately 60% for the

temperature of 800 °C. The maximum difference in toughness index ratio between Q690 and S690 steel was 40% for the temperature of 400 °C. The high-strength steel with the same strength grade but different categories may demonstrate different fracture resistance after being exposed to the same high temperature. This deviation in toughness index between Chinese (Q) and European (S) steels may be caused by several factors such as the divergences of exposure temperature and cooling rate in the post-fire material tests and the variety of material properties due to different production processes.

Fig. 22(c) and 20(d) illustrates the representative comparison of damage evolution law curves of 460 and 690 steels after being exposed to high temperatures. When the experienced temperature was no more than 500 °C, for the same experienced temperature and plastic displacement, the developed damage index of Q460 steel was smaller than that of S460. When the experienced temperature was higher than 500 °C, the opposite was found. For Q690 and S690 steels, only when the experienced temperature was 800 °C, the developed damage index of Q690 steel was larger than that of S690 steel at a given plastic displacement. The quite different damage evolution behavior after high temperature exposure for high-strength steels may be also caused by variety of material properties and the divergences of temperature and cooling rate during the post-fire tests. However, more metallurgical analyses are needed to explore this divergence.

5. Recommendation for numerical prediction of post-fire fracture behavior of high-strength steels

The post-necking material properties listed in Tables 1 to 15 has been validated for fracture prediction of high-strength steels (Q460, Q550, Q690, Q890, S460, S690, S960) after exposure to high temperatures. To simplify the material properties for fracture prediction, the recommended post-necking material properties for fracture prediction of the high-strength steels were summarized in Tables 16 and 17. The proposed

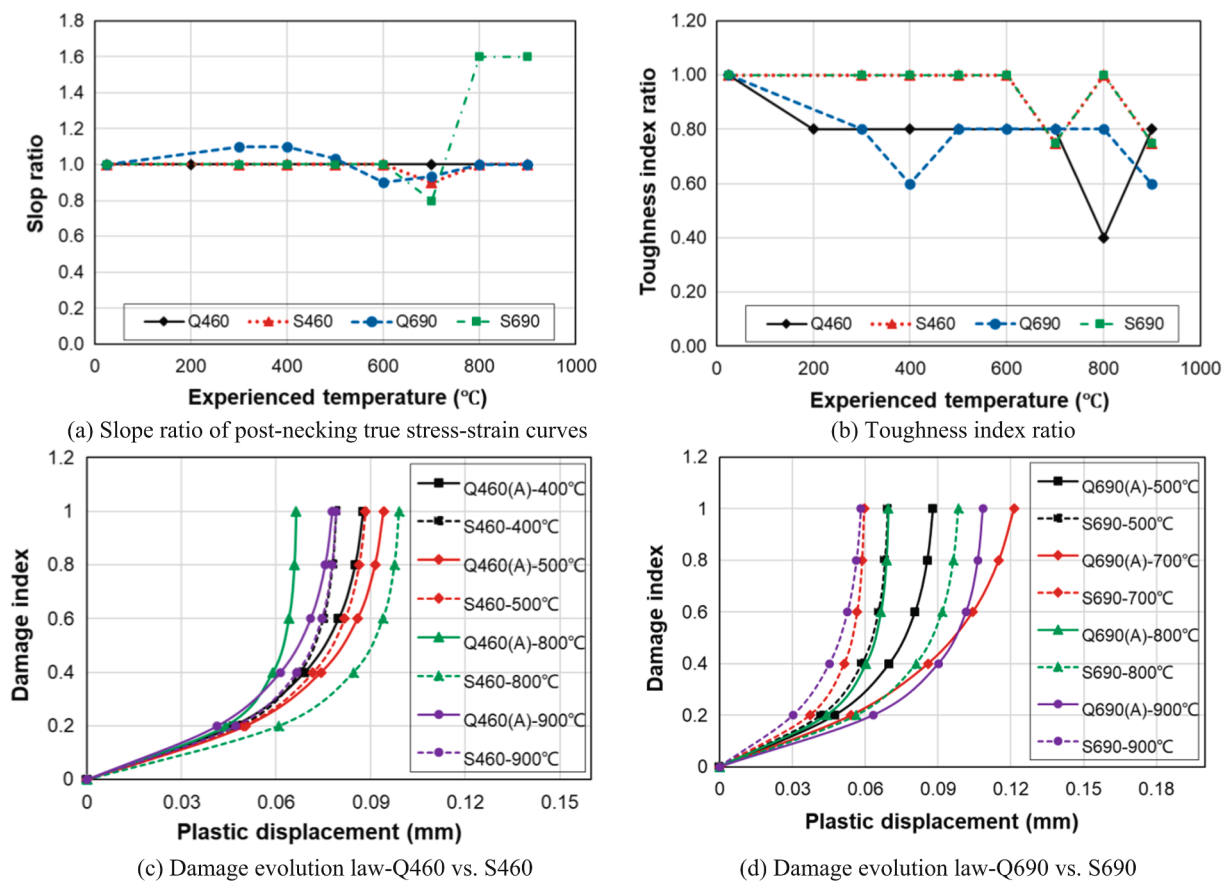


Fig. 22. Comparison of post-necking material properties for the high-strength steels with same yield strength.

Table 16

Recommended post-necking material properties for fracture prediction of Q460-Q890 and S460-S960 steels after fire (air-cooling condition).

Material properties	Temperature	Q460	Q550	Q690	Q890	S460	S690	S960	
Slope ratio of post-necking true stress-strain curves	$20^{\circ}\text{C} < T \leq 400^{\circ}\text{C}$	1.0	1.1	1.1	1.1	1.0	1.0	1.0	
Initial slope = 690 MPa (Q460, Q550, Q690, Q890, S460)	$400^{\circ}\text{C} < T \leq 600^{\circ}\text{C}$	1.0	1.0	1.0	1.2	1.0	1.0	1.0	
Initial slope = 345 MPa (S690, S960)	$600^{\circ}\text{C} < T \leq 800^{\circ}\text{C}$	1.0	1.0	1.0	1.3	0.8	0.5	0.8	
	$800^{\circ}\text{C} < T \leq 900^{\circ}\text{C}$	1.0	0.5	0.5	1.4	1.0	1.5	1.5	
Toughness index ratio	$20^{\circ}\text{C} < T \leq 400^{\circ}\text{C}$	0.8	0.8	0.6	0.6	1.0	1.0	0.75	
Initial toughness index = 2.5 (Q460-Q890)	$400^{\circ}\text{C} < T \leq 600^{\circ}\text{C}$	0.8	0.8	0.8	0.8	1.0	1.0	1.0	
Initial toughness index = 2.0 (S460-S960)	$600^{\circ}\text{C} < T \leq 800^{\circ}\text{C}$	0.4	0.8	0.8	0.8	0.5	0.75	0.5	
	$800^{\circ}\text{C} < T \leq 900^{\circ}\text{C}$	0.8	0.8	0.6	0.8	0.75	0.75	0.25	
Parameters of damage evolution law	$20^{\circ}\text{C} < T \leq 400^{\circ}\text{C}$	u_o	0.09	0.1	0.06	0.07	0.08	0.07	0.05
		k	3.5	3.5	7.0	6.0	4.5	4.5	6.0
	$400^{\circ}\text{C} < T \leq 600^{\circ}\text{C}$	u_o	0.09	0.1	0.09	0.07	0.08	0.06	0.06
		k	3.5	3.5	3.0	5.5	4.0	4.5	5.5
	$600^{\circ}\text{C} < T \leq 800^{\circ}\text{C}$	u_o	0.07	0.1	0.07	0.05	0.07	0.04	0.04
		k	5.5	3.5	3.0	5.5	5.0	4.5	5.5
	$800^{\circ}\text{C} < T \leq 900^{\circ}\text{C}$	u_o	0.08	0.1	0.07	0.07	0.08	0.06	0.04
		k	3.5	3.5	4.5	7.0	4.5	3.5	6.0

material properties were based on the initial properties without experiencing high temperature. The initial slope of post-necking true stress-strain curve was assumed to be 690 MPa (Q460-Q890 and S460) and 345 MPa (S690 and S960), respectively. The initial toughness index was assumed to 2.5 (Q460-Q890) and 2.0 (S460-S960). The fracture parameter β in SMCS model was assumed to be 2.0. For the damage evolution law, it was assumed that the characteristic length of element was 1.0 mm when calibrating the plastic displacement. These material properties may conservatively predict the overall deformation capacity and the fracture behavior of high-strength steel tension specimen.

6. Conclusions

This study proposed a fracture prediction approach for high-strength steels including Chinese high-strength steels (Q460, Q550, Q690, Q890) and European high-strength steels (S460, S690, S890) in tension after being exposed to temperature ranging from 20 to 900°C and cooled by different methods (air and water). The post-necking material properties for post-fire fracture prediction such as post-necking true stress-strain curves, toughness index in SMCS model and damage evolution law were investigated and proposed for these high-strength steels. The proposed material properties of these high-strength steels can be used for predicting the fracture caused by high stress triaxiality and provide

Table 17

Recommended post-necking material properties for fracture prediction of Q460-Q890 (water-cooling condition).

Material properties	Temperature	Q460	Q550	Q690	Q890	
Slope ratio of post-necking true stress-strain curves	20 °C < T ≤ 400 °C	1.0	1.1	1.1	1.1	
Initial slope = 690 MPa (Q460, Q550, Q690, Q890, S460)	400 °C < T ≤ 600 °C	1.0	1.1	1.0	1.2	
Initial slope = 345 MPa (S690, S960)	600 °C < T ≤ 800 °C	1.0	1.0	1.0	1.3	
Toughness index ratio	800 °C < T ≤ 900 °C	1.0	0.5	0.5	1.4	
Initial toughness index = 2.5 (Q460-Q890)	20 °C < T ≤ 400 °C	0.8	0.8	0.6	0.6	
Initial toughness index = 2.0 (S460-S960)	400 °C < T ≤ 600 °C	0.8	0.8	0.2	0.6	
Parameters of damage evolution law	600 °C < T ≤ 800 °C	0.4	0.4	0.2	0.4	
	800 °C < T ≤ 900 °C	0.6	0.6	0.6	0.6	
	20 °C < T ≤ 400 °C	u_o k	0.10 4.0	0.08 3.5	0.07 4.0	0.07 6.0
	400 °C < T ≤ 600 °C	u_o k	0.09 4.0	0.09 4.0	0.03 6.0	0.07 5.5
	600 °C < T ≤ 800 °C	u_o k	0.09 3.0	0.06 4.0	0.07 3.0	0.05 5.0
	800 °C < T ≤ 900 °C	u_o k	0.11 2.5	0.06 6.0	0.07 6.0	0.07 6.0

conservative estimation of their fracture behavior including fracture resistance and damage evolution after fire. The following conclusions can be drawn:

- 1) Chinese and European high-strength steels with similar strength grade may exhibit different fracture behavior after being exposed to similar high temperatures. Therefore, it is quite necessary to choose reasonable post-fire material properties for fracture prediction of different high strength steels.
- 2) True stress-strain curves after onset of necking can be simply expressed by a straight line with a slope for high strength steels after being exposed to high temperatures. The slope can affect the softening of material after onset of necking and the damage index in material. Compared with Q890 steels, the slope of Q460, Q550, Q690 steels was less sensitive to the experienced temperature. For S460, S690 and S960 steels, the post-necking slope of true stress-strain curves was only affected after they were exposed to a temperature higher than 600 °C.
- 3) The toughness index in SMCS model is a measure of resistance to fracture initiation in material. The Q460-Q890 steels experienced maximum reduction in toughness index after being exposed to temperatures between 800 °C and 900 °C, which is defined as critical temperature range. For S460-S960 steels, the critical temperature range was from 750°C to 900 °C.
- 4) The damage evolution law describes the damage development in material caused by fracture initiation and propagation. A rapid evolution of damage can lead to a lower toughness index and plastic deformation at failure. For these high-strength steels, the most rapid evolution of damage occurs after being exposed to temperatures in a range of 650 °C to 900 °C.
- 5) The fracture behavior of high-strength steels was significantly affected by cooling methods. The slope of post-necking true stress-strain curves decreased greatly (by 50%) when using water-cooling method, but was practically invariant for air-cooling method. The maximum reduction (by 80%) in toughness index was more significant for the watering-cooling method than that using air-cooling

method. The water-cooling method may even lead to a brittle fracture mode of high-strength steels, for which the toughness index was nearly 0.2.

- 6) This study summarized the variation of the post-necking material properties of high-strength steels with the exposed temperatures and cooling methods. However, more metallurgical analyses for high-strength steels after fire are still needed to obtain the details of steel compositions, grain size and inclusions for high-strength steels after fire and to obtain the scientific basis for these variation trends.

CRediT authorship contribution statement

Wen-Yu Cai: Conceptualization, Methodology, Writing - original draft. **Jian Jiang:** Investigation, Formal analysis, Visualization. **Yan-Bo Wang:** Validation, Funding acquisition. **Guo-Qiang Li:** Validation, Supervision.

Declaration of Competing Interest

The authors declare that they have no known competing financial interests or personal relationships that could have appeared to influence the work reported in this paper.

Acknowledgement

Financial support by the National Natural Science Foundation of China (Project No. 52008313) is greatly acknowledged.

References

- [1] Wang Y-Z, Li G-Q, Wang Y-B, Lyu Y-F, Li H. Ductile fracture of high strength steel under multi-axial loading. Eng Struct 2020;210:110401. <https://doi.org/10.1016/j.engstruct.2020.110401>.
- [2] Jiang J, Ye ZJ, Bao W, Wang X, Wang YB, Dai XH. Flexural buckling behaviour of 690 MPa high strength steel H-section columns. Eng Struct 2019;200:109718. <https://doi.org/10.1016/j.engstruct.2019.109718>.
- [3] Sajid HU, Kiran R. Post-fire mechanical behavior of ASTM A572 steels subjected to high stress triaxialities. Eng Struct 2019;191:323–42.
- [4] Sajid HU, Naik DL, Kiran R. Microstructure–Mechanical Property Relationships for Post-Fire Structural Steels. J Mater Civ Eng 2020;32(6):04020133. [https://doi.org/10.1061/\(ASCE\)MT.1943-5533.0003190](https://doi.org/10.1061/(ASCE)MT.1943-5533.0003190).
- [5] Kanvinde AM, Deierlein GG. Void growth model and stress modified critical strain model to predict ductile fracture in structural steels. J Struct Eng 2006;132(12): 1907–18. [https://doi.org/10.1061/\(ASCE\)0733-9445\(2006\)132:12\(1907\)](https://doi.org/10.1061/(ASCE)0733-9445(2006)132:12(1907)).
- [6] Qiang XH, Bijlaard F, Kolstein H. Dependence of mechanical properties of high strength structural steel S690 on elevated temperatures. Constr Build Mater 2012; 30:73–9. <https://doi.org/10.1016/j.conbuildmat.2011.12.018>.
- [7] Qiang X, Bijlaard FSK, Kolstein H. Elevated-temperature mechanical properties of high strength structural steel S460N: Experimental study and recommendations for fire-resistance design. Fire Saf J 2013;55:15–21.
- [8] Qiang X, Jiang Xu, Bijlaard FSK, Kolstein H. Mechanical properties and design recommendations of very high strength steel S960 in fire. Eng Struct 2016;112: 60–70.
- [9] Xiong MX, Liew JYR. Experimental study to differentiate mechanical behaviours of TMCP and QT high strength steel at elevated temperatures. Constr Build Mater 2020;242:118105. <https://doi.org/10.1016/j.conbuildmat.2020.118105>.
- [10] Chen J, Young B, Uy B. Behavior of High Strength Structural Steel at Elevated Temperatures. J Struct Eng 2006;132(12):1948–54.
- [11] Wang W, Wang K, Kodur V, Wang B. Mechanical Properties of High-Strength Q690 Steel at Elevated Temperature. J Mater Civ Eng 2018;30(5):04018062. [https://doi.org/10.1061/\(ASCE\)MT.1943-5533.0002244](https://doi.org/10.1061/(ASCE)MT.1943-5533.0002244).
- [12] Huang L, Li GQ, Wang XX, Zhang C, Choe L, Engelhardt MD. High temperature mechanical properties of high strength structural steels Q550, Q690 and Q890. Fire Technol 2018;54(6):1609–28. <https://doi.org/10.1007/s10694-018-0765-4>.
- [13] Jiang J, Bao W, Peng ZY, Wang YB, Liu J, Dai XH. Experimental investigation on mechanical behaviours of TMCP high strength steel. Constr Build Mater 2019;200: 664–80.
- [14] Smith CL, Kirby BR, Lapwood DG, Cole KJ, Cunningham AP, Preston RR. The reinstatement of fire damaged steel framed structures. Fire Saf J 1981;4(1):21–62.
- [15] Outinen J. Mechanical properties of structural steels at high temperature and after cooling down. Ph.D. dissertation. Helsinki, Finland: Helsinki University of Technology; 2007.
- [16] Qiang X, Bijlaard FSK, Kolstein H. Post-fire mechanical properties of high strength structural steels S460 and S690. Eng Struct 2012;35:1–10.
- [17] Qiang X, Bijlaard FSK, Kolstein H. Post-fire mechanical properties of very high strength steel S960. J Constr Steel Res 2013;80:235–42. <https://doi.org/10.1016/j.jcsr.2012.09.002>.

- [18] Chiew SP, Zhao MS, Lee CK. Mechanical properties of heat-treated high strength steel under fire/post-fire conditions. *J Constr Steel Res* 2014;98:12–9.
- [19] Gunalan S, Mahendran M. Experimental investigation of post-fire mechanical properties of cold-formed steels. *Thin-Walled Struct* 2014;84:241–54.
- [20] Aziz EM, Kodur VK. Effect of temperature and cooling regime on mechanical properties of high-strength low-alloy steel: Mechanical Properties of HSLA steel at elevated temperatures. *Fire Mater* 2016;40(7):926–39.
- [21] Lee J, Engelhardt M, Taleff ME. Mechanical properties of ASTM A992 steel after fire. *Eng J* 2012;49(1):33–44. <https://doi.org/10.3744/SNAK.2012.49.1.33>.
- [22] Lu J, Liu H, Chen Z, Liao X. Experimental investigation into the post-fire mechanical properties of hot-rolled and cold-formed steels. *J Constr Steel Res* 2016;121:291–310.
- [23] Zhang YJ, Zhu Y, Zhao S, Hu KX. Experimental research on mechanical properties of steel cooled in different modes after high temperature treatment. *Struct Eng* 2009;25(5):104–9.
- [24] Sajid HU, Kiran R. Influence of stress concentration and cooling methods on post-fire mechanical behavior of ASTM A36 steels. *Constr Build Mater* 2018;186:920–45.
- [25] Wang W, Liu T, Liu J. Experimental study on post-fire mechanical properties of high strength Q460 steel. *J Constr Steel Res* 2015;114:100–9.
- [26] Zhou H, Wang W, Wang K, Xu L. Mechanical properties deterioration of high strength steels after high temperature exposure. *Constr Build Mater* 2019;199:664–75.
- [27] Li GQ, Lyu H, Zhang C. Post-fire mechanical properties of high strength Q690 structural steel. *J Constr Steel Res* 2017;132:108–16.
- [28] Wang F, Lui EM. Experimental study of the post-fire mechanical properties of Q690 high strength steel. *J Constr Steel Res* 2020;167:105966. <https://doi.org/10.1016/j.jcsr.2020.105966>.
- [29] Azhari F, Heidarpour A, Zhao X-L, Hutchinson CR. Mechanical properties of ultra-high strength (Grade 1200) steel tubes under cooling phase of a fire: An experimental investigation. *Constr Build Mater* 2015;93:841–50.
- [30] McClintock F. A criterion for ductile fracture by the growth of holes. *J Appl Mech* 1968;35(2):363–71. <https://doi.org/10.1115/1.3601204>.
- [31] Rice JR, Tracey DM. On the ductile enlargement of voids in triaxial stress fields*. *J Mech Phys Solids* 1969;17(3):201–17.
- [32] Hancock JW, Mackenzie AC. On the mechanisms of ductile failure in high-strength steels subjected to multi-axial stress-states. *J Mech Phys Solids* 1976;24(2-3):147–60.
- [33] Cockcroft M, Latham D. Ductility and the workability of metals. *Journal Institute of Metals* 1968;68:33–9.
- [34] Gurson AL. Continuum Theory of Ductile Rupture by Void Nucleation and Growth: Part I—Yield Criteria and Flow Rules for Porous Ductile Media. *J Eng Mater Technol-Trans ASME* 1977;99(1):2–15. <https://doi.org/10.1115/1.3443401>.
- [35] Johnson GR, Cook WH. Fracture characteristics of three metals subjected to various strains, strain rates, temperatures and pressures. *Eng Fract Mech* 1985;21(1):31–48.
- [36] Bao Y, Wierzbicki T. On fracture locus in the equivalent strain and stress triaxiality space. *Int J Mech Sci* 2004;46(1):81–98.
- [37] Li W, Liao F, Zhou T, Askes H. Ductile fracture of Q460 steel: Effects of stress triaxiality and Lode angle. *J Constr Steel Res* 2016;123:1–17.
- [38] Xiang P, Jia LJ, Ke Ke, Chen Y, Ge H. Ductile cracking simulation of uncracked high strength steel using an energy approach. *J Constr Steel Res* 2017;138:117–30.
- [39] Kang L, Ge H, Suzuki M, Wu Bo. An average weight whole-process method for predicting mechanical and ductile fracture performances of HSS Q690 after a fire. *Constr Build Mater* 2018;191:1023–41.
- [40] Guo W, Crowther D, Francis JA, Thompson A, Liu Z, Li L. Microstructure and mechanical properties of laser welded S960 high strength steel. *Mater Des* 2015;85:534–48.
- [41] GB/T228.1-2010, Metallic Materials Ensil Testing. 1: Method of Test at Room Temperature, China Standard Press, Beijing, 2010.
- [42] ABAQUS User's Manual. Hibbit, Karlsson, & Sorensen, Inc., Pawtucket, RI.
- [43] Cai W. Steel Fracture Modelling at Elevated Temperature for Structural-Fire Engineering Analysis. (Ph.D. Thesis). Department of Civil, Architectural, and Environmental Engineering, University of Texas at Austin, Austin, TX, 2015.
- [44] Zhou MW, Yu H. Effects of precipitates and inclusions on the fracture toughness of hot rolling X70 pipeline steel plates. *Int J Miner Metall Mater* 2012;19(9):805–11.
- [45] Azhari F, Heidarpour A, Zhao X-L, Hutchinson CR. Post-fire mechanical response of ultra-high strength (Grade 1200) steel under high temperatures: Linking thermal stability and microstructure. *Thin-Walled Struct* 2017;119:114–25.
- [46] ASTM E8/E8M, Standard test methods for tensile testing of metallic materials, 2016.
- [47] Li G.Q., Lyu H., Zhang C. Post-fire mechanical properties of high strength Q550 structural steel. The 11th Pacific Structural Steel Conference (PSSC'16), 2016: 1410–1416.
- [48] Lyu H. Post-fire mechanical properties of high strength structural steel over 500 MPa (Master's thesis). Department of Civil Engineering, Tongji University, Shanghai, China 2017.